





ARTICLE

# An APP ectodomain mutation outside of the A $\beta$ domain promotes A $\beta$ production in vitro and deposition in vivo

Xulun Zhang<sup>1</sup>, Can Martin Zhang<sup>2</sup>, Dmitry Prokopenko<sup>2</sup>, Yingxia Liang<sup>2</sup>, Sherri Y. Zhen<sup>2</sup>, Ian Q. Weigle<sup>1</sup>, Weinong Han<sup>1</sup>, Manish Aryal<sup>1</sup>, Rudolph E. Tanzi<sup>2</sup>, and Sangram S. Sisodia<sup>1</sup>

**Familial Alzheimer’s disease (FAD)–linked mutations in the APP gene occur either within the A $\beta$ -coding region or immediately proximal and are located in exons 16 and 17, which encode A $\beta$  peptides. We have identified an extremely rare, partially penetrant, single nucleotide variant (SNV), rs145081708, in APP that corresponds to a Ser198Pro substitution in exon 5. We now report that in stably transfected cells, expression of APP harboring the S198P mutation (APPS198P) leads to elevated production of A $\beta$  peptides by an unconventional mechanism in which the folding and exit of APPS198P from the endoplasmic reticulum is accelerated. More importantly, coexpression of APP S198P and the FAD-linked PS1 $\Delta$ E9 variant in the brains of male and female transgenic mice leads to elevated steady-state A $\beta$  peptide levels and acceleration of A $\beta$  deposition compared with age- and gender-matched mice expressing APP and PS1 $\Delta$ E9. This is the first AD-linked mutation in APP present outside of exons 16 and 17 that enhances A $\beta$  production and deposition.**

## Introduction

Alzheimer’s disease (AD) is a progressive neurodegenerative disease that is pathologically characterized by the extracellular deposition of amyloid  $\beta$  (A $\beta$ ) peptides in senile plaques and the intraneuronal accumulation of hyperphosphorylated forms of Tau (Glennner and Wong, 1984; Hardy and Allsop, 1991; Masters et al., 1985; Price et al., 1998). A $\beta$  peptides of between 40 and 43 amino acids in length are generated by the sequential proteolysis of the amyloid precursor protein (APP) by BACE1 and the  $\gamma$ -secretase complex (De Strooper and Annaert, 2000; Vassar et al., 1999; Wolfe, 2020). APP is a type I transmembrane protein that is encoded by alternatively spliced mRNAs encoded by the APP gene on chromosome 21 (De Strooper and Annaert, 2000; Price et al., 1998). Rare, autosomal dominant familial forms of AD (FADs) are caused by inheritance of mutations in genes encoding APP and presenilins (PS1 and PS2; see <https://www.alzforum.org/mutations>). Mutations in the APP gene are located in exons 16 and 17, which encode 17 and 23–26 amino acids, respectively, of the A $\beta$  peptide. These mutations occur either within the A $\beta$ -coding region (“Flemish,” “Arctic,” “Dutch,” “Iowa,” “Tottori,” and “English” variants) or immediately proximal (“Swedish” mutation and mutations between amino acids 714 and 724; 770 numbering; see Fig. 1 A; Van

Broeckhoven and Kumar-Singh, 2006). Depending on the nature of the mutation, the encoded APP variants undergo differential processing that leads to elevated levels of all A $\beta$  peptide species, as is observed with the APP Swedish variant (Citron et al., 1992; Haass et al., 1995; Thinakaran et al., 1996) or elevations in the ratio of A $\beta$ 42 to A $\beta$ 40 peptides that are promoted by numerous mutations at amino acids 714–724 within the APP transmembrane domain (De Jonghe et al., 2001). Mutations within the A $\beta$  domain alter the biophysical properties of the A $\beta$  peptide variants in a manner that increases the nucleation and fibrillization of these polypeptides (Hunter and Brayne, 2018; Kumar-Singh et al., 2000). Moreover, mutations in the presenilins also lead to elevations in the ratio of A $\beta$ 42/A $\beta$ 40 peptides (De Strooper, 2007), suggesting that nucleation-prone A $\beta$ 42 peptides are the pathogenic drivers of A $\beta$  amyloidosis.

In a search for AD-associated rare variants, we identified a novel missense mutation in APP corresponding to a Ser198Pro amino acid substitution that was present in both affected siblings from one family in the National Institute of Mental Health (NIMH) AD Genetics Initiative Family Sample (with no unaffected siblings available). At the time, this missense mutation was not present in any available genetic database, but was later

<sup>1</sup>Department of Neurobiology, University of Chicago, Chicago, IL; <sup>2</sup>Department of Neurology, Genetics and Aging Research Unit, MassGeneral Institute for Neurodegenerative Diseases, Massachusetts General Hospital, Charlestown, MA.

Correspondence to Sangram S. Sisodia: [ssisodia@bsd.uchicago.edu](mailto:ssisodia@bsd.uchicago.edu); Rudolph E. Tanzi: [tanzi@helix.mgh.harvard.edu](mailto:tanzi@helix.mgh.harvard.edu).

© 2021 Zhang et al. This article is distributed under the terms of an Attribution–Noncommercial–Share Alike–No Mirror Sites license for the first six months after the publication date (see <http://www.rupress.org/terms/>). After six months it is available under a Creative Commons License (Attribution–Noncommercial–Share Alike 4.0 International license, as described at <https://creativecommons.org/licenses/by-nc-sa/4.0/>).

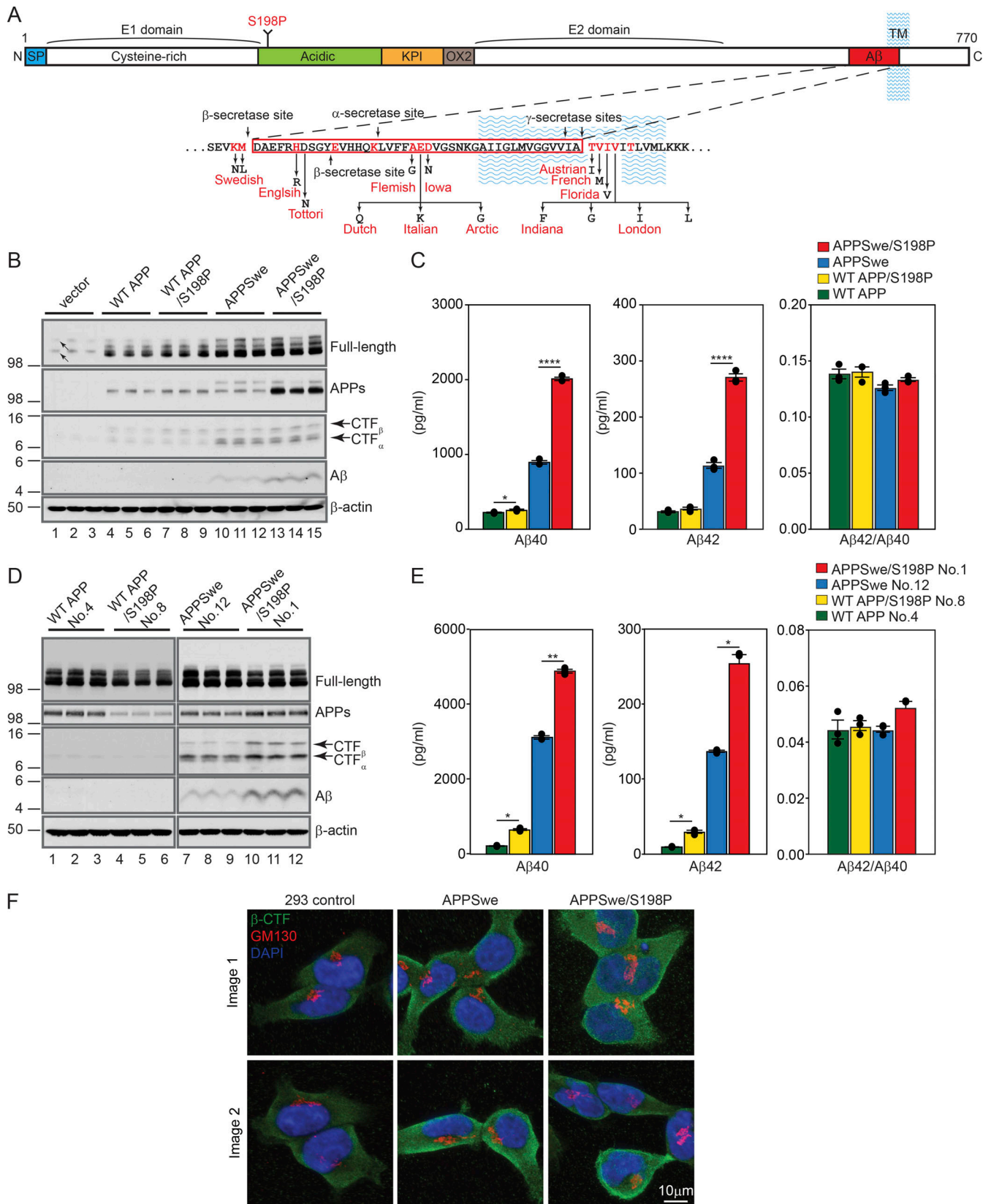


Figure 1. **Impact of S198P on Aβ production in HEK293 cells.** (A) Domain organization of APP-770, positions of FAD-linked mutations and Serine 198. Shown are the domains of APP and positions of the FAD-linked mutations in exons 16 and 17. The S198 mutation is in the linker between the E1 domain and acidic-rich domain. (B and D) Western blot analysis of full-length APP and APP CTFs in cell lysates and soluble APP and Aβ in CM of the HEK293 cell pools (B) and cell lines (D) stably expressing WT APP, WT APP695/S198P, APP695Swe, and APP695Swe/S198P, and the lysates and CM were prepared from triplicate

wells of culture plates. Equal amounts of cell lysates and normalized volumes of CM based on the protein concentrations of the cell lysates were used for the analysis. Small arrows in vector transfected cells (B) indicate the migration of endogenous full-length APP. **(C and E)** MSD analysis of A $\beta$  levels in the CM of the stable cell pools (C) and cell lines (E). Levels of A $\beta$  species were normalized to the protein concentrations of the cell lysates. The results are represented by mean  $\pm$  SEM, and the error bars represent SEM,  $n = 3$ . One-way ANOVA with a Tukey's multiple comparisons post hoc test was used to establish statistical significance. \*,  $P < 0.05$ ; \*\*,  $P < 0.005$ ; \*\*\*,  $P < 0.0001$ . **(F)** Subcellular distribution of  $\beta$ -CTF in APPSwe no. 12 and APPSwe/S198P no. 1 cells. Immunofluorescence images of 3D6-immunoreactive  $\beta$ -CTF (green) and colabeled Golgi-specific GM130 (red). DAPI is in blue. Each column contains two images acquired from different fields (top and bottom) of the same dish. KPI, Kunitz protease inhibitor.

reported as an extremely rare single nucleotide variant (SNV), rs145081708, with a minor allele frequency ranging from 0.000382 (TOPMED,  $n = 125,568$ ) to 0.000684 (GnomAD\_exome,  $n = 251,438$ ). Over the course of our functional studies, rs145081708 was also reported in ClinVar (public database of clinical variant interpretations; Landrum et al., 2018) in four separate submissions, which concluded these variants were “benign” or “of uncertain significance.” Recently, the rs145081708 SNV encoding the APP-Ser198Pro mutation was also reported in an Ashkenazi Jewish family with monozygotic triplets, of whom two of the triplets were affected with AD and one, at the age of 85 yr, had no cognitive complaints, thus suggesting that the SNV is partially penetrant (Zhang et al., 2019a). Notably, both affected triplets carried the proline mutation, with onset age and Apolipoprotein E (ApoE;  $\epsilon$ ) status 73 yr ( $\epsilon 3/\epsilon 4$ ) and 76 yr ( $\epsilon 3/\epsilon 4$ ). Additionally, an offspring of one of the affected triplets was a carrier of S198P and had early-onset AD (EOAD; age of onset at 50 yr and  $\epsilon 3/\epsilon 4$ ).

As serine 198 is encoded in exon 5 and hence is remote from the A $\beta$  sequence (see Fig. 1 A), we considered it highly unlikely that this mutation could directly influence BACE1 and  $\gamma$ -secretase processing of APP to generate A $\beta$  peptides. However, S198 is one of two phosphorylation sites in the extracellular domain (Walter et al., 1997), and introduction of an experimental mutation at the second site (S206G) has been reported to reduce cell surface levels of this APP mutant (Zhang et al., 2019b). However, the influence of the S198P mutation on APP trafficking, posttranslational modifications, proteolytic processing, A $\beta$  production, and pathogenesis has not been determined. To address these issues, we have examined the effects of the S198P mutation on APP metabolism both in stably transfected cultured mammalian cells and in the brains of transgenic mice expressing this APP variant. The S198P mutation was engineered into a mouse APP-695 cDNA wherein the A $\beta$  region was replaced with sequences encoding human A $\beta$  (there are three amino acid differences between mouse and human A $\beta$  peptides) as well as into cDNA encoding chimeric APP695 that also harbors the FAD-linked Swedish lysine-methionine to asparagine-leucine (KM-NL) mutations that promote cleavage by BACE1 and hence facilitate detection of A $\beta$  peptide species (Borchelt et al., 1996b). We now report that expression of the APP695/S198P or APP695Swe/S198P variants leads to elevated levels of A $\beta$  peptides in the conditioned medium (CM) of transfected cells compared with A $\beta$  peptide levels in the CM of cells in which APP695 or APP695Swe, respectively, are expressed at similar levels. Our cell biological studies reveal that enhanced production of A $\beta$  from cells expressing the APP695Swe/S198P variant is the result of enhanced rate of folding and exit of these polypeptides from the ER. To establish the in vivo relevance of these

findings and to assess the role of the S198P mutation on promoting A $\beta$  amyloidosis, we generated transgenic mice that express this APP variant. We now show that the steady-state levels of A $\beta$ 40 and A $\beta$ 42 in brains of male or female APP695Swe/S198P transgenic mice that coexpress the FAD-linked PS1 $\Delta$ E9 variant that elevates A $\beta$ 42/40 ratio and accelerates A $\beta$  deposition in transgenic mice (Jankowsky et al., 2004) are significantly elevated compared with age- and gender-matched mice that coexpress APP695Swe and PS1 $\Delta$ E9. More importantly, A $\beta$  deposition in the brains of male or female transgenic mice at 4, 6, or 9 mo is markedly elevated compared with gender-matched transgenic mice that coexpress APP695Swe and PS1 $\Delta$ E9. These studies unequivocally demonstrate that the S198P mutation in exon 5 leads to enhanced production of A $\beta$  peptides that accelerate A $\beta$  deposition in vivo. Thus, this is the first AD-linked mutation in APP present outside of exons 16 and 17 that affects A $\beta$  production and deposition in vivo and thus challenges the conventional wisdom that APP mutations outside of exons 16 and 17 that are identified in patients with AD are “benign” or “of uncertain significance” (Nicolas et al., 2016; Sassi et al., 2014).

## Results

### Genetic studies that identify the APP S198P variant

Analysis of whole genome sequencing (WGS) of the NIMH AD Genetics Initiative Family Sample (Prokopenko et al., 2020) revealed a novel missense mutation in APP corresponding to a Ser198Pro amino acid substitution, which was present in both affected siblings from one family with no unaffected siblings available. The first affected sibling was 59 yr old at onset of AD and was homozygous for APOE- $\epsilon 4$ . The second sibling was 68 yr old at onset and was APOE- $\epsilon 3/\epsilon 4$ .

The APP-Ser198Pro mutation was later reported as the extremely rare SNV, rs145081708, with a minor allele frequency ranging from 0.000382 (TOPMED,  $n = 125,568$ ) to 0.000684 (GnomAD\_exome,  $n = 251,438$ ), and in ClinVar in four separate submissions, two of which describe the amino acid change as “benign” and two as “of uncertain significance.” We also evaluated two other large WGS AD datasets described in Table S1. Data regarding the NIMH and National Institute on Aging (NIA) samples have been described elsewhere (Beecham et al., 2017; Blacker et al., 1997). Family-based cohorts analyzed consisted of multiplex AD families with affected and unaffected siblings. In the NIA Alzheimer's Disease Sequencing Project (ADSP) families, we found one unaffected carrier with this SNV. The subject's age at last examination and APOE status were 77 yr and  $\epsilon 3/\epsilon 3$ , respectively. No subjects in the NIA family sample carried the mutation. In the NIA ADSP case-control cohort of unrelated individuals, we found one affected carrier and two unaffected

carriers. The affected carrier's age at onset was 60 yr, and the APOE status was  $\epsilon 2/\epsilon 4$ . Both unaffected subjects carried one APOE- $\epsilon 4$  allele and were 72 and 82 yr old, respectively, at last examination. The small number of total carriers of the minor allele of rs145081708 (APP-198Pro) in all three datasets was not sufficient to carry out a formal statistical test.

### Stable expression of APP695 harboring the S198P mutation enhances A $\beta$ production

To examine the metabolism of APP harboring the S198P mutation, we generated stable cell "pools" that constitutively express either WT human APP695 (APP695) or human APP695 with the S198P mutation (APP695/S198P). Cell lysates and CM from stable cell pools were fractionated on Tris-Tricine gels and subjected to Western blot analysis (Fig. 1 B). The levels of full-length APP and APP-C-terminal fragments (CTFs) were similar in lysates from cell pools expressing either APP695 or APP695/S198P, and A $\beta$  levels in the CM were detectable, albeit at very low levels (Fig. 1 B, lanes 4–9). Using a highly sensitive and quantitative Meso Scale Discovery (MSD) assay, we observed that A $\beta$ 40 in the CM of cell pools expressing APP695/S198P were  $\sim 1.2$  times higher than A $\beta$  levels in the CM of cells expressing APP695 (Fig. 1 C). To facilitate detection of A $\beta$ , the S198P mutation was introduced into human APP695 cDNA that harbors the FAD-linked Swedish variant (KM-NL; APPSwe) that leads to enhanced processing by BACE1 and ultimately to elevated A $\beta$  production (Citron et al., 1992), and cell pools were generated that express either APP695Swe/S198P or APP695Swe. The levels of full-length APP between the cell pools expressing APP695Swe or APP695Swe/S198P were comparable, but compared with cell pools expressing APP695Swe, the levels of cellular APP-CTFs and secreted A $\beta$  were significantly elevated in the cell pools expressing APP695Swe/S198P (Fig. 1 B; compare lanes 10–12 to lanes 13–15, respectively). MSD-A $\beta$  analysis confirmed an approximately twofold increase in A $\beta$ 40 and A $\beta$ 42 peptides in the CM of the APP695Swe/S198P cell pools compared with A $\beta$  levels in the cell pools expressing APP695Swe (Fig. 1 C).

In parallel, we isolated individual cell lines that stably express APP695, APP695/S198P, APP695Swe, or APP695Swe/S198P. Stable cell lines with matching expression for each pairwise comparison were identified by Western blot analysis and expanded. As was the case in the stable cell pools, A $\beta$  in the CM of APP695 line no. 4 and APP695/S198P line no. 8 was barely detectable by Western blotting (Fig. 1 D, lanes 1–6), but MSD-A $\beta$  analysis revealed that the CM of APP695/S198P no. 8 contained approximately twofold higher levels of A $\beta$ 40 and A $\beta$ 42 than the CM of APP695 no. 4 (Fig. 1 E). Similarly, the levels of cellular full-length APP695Swe in line no. 12 and APP695Swe/S198P in line no. 1 were comparable, but compared with the levels of cellular APP CTFs and secreted A $\beta$  in the CM of APP695Swe no. 12 cells, APP695Swe/S198P no. 1 cells exhibited substantially higher levels of these APP derivatives (Fig. 1 D; compare lanes 7–9 to 10–12, respectively). MSD-A $\beta$  analysis confirmed an  $\sim 1.8$ -fold elevation in levels of both A $\beta$ 40 and A $\beta$ 42 in CM of APP695Swe/S198P no. 1 compared with APP695Swe no. 12 (Fig. 1 D, lanes 7–12; Fig. 1 E). To assess the possibility that differential trafficking or accumulation of  $\beta$ -CTF derived from APPSwe or

APPSwe/S198P might explain the differences in A $\beta$  production, we performed immunofluorescence staining on APPSwe line no. 12 and APPSwe/S198P line no. 1 using a recombinant mouse antibody, 3D6, a neo-epitope-specific antibody recognizing A $\beta$  residues 1–5 with strong preference for an exposed aspartate residue at the N terminus of the peptide (Bacskai et al., 2001; Johnson-Wood et al., 1997; Kamenetz et al., 2003). This antibody does not react with full-length APP or APP-CTF $\alpha$  (Kim et al., 2001). While very low levels of staining were detected in naive HEK293 cells using conventional indirect immunofluorescence and light microscopy, we failed to detect any significant differences in the steady-state distributions of  $\beta$ -CTF in reticular, vesicular, or sub-plasma membrane compartments between APPSwe and APPSwe/S198P cells (Fig. 1 F).

Taken together, these studies confirm that in stably transfected HEK293 cells, the APP S198P mutation enhances A $\beta$  production compared with cells expressing parental APP.

### Metabolism of the APPS198P variant and influences on A $\beta$ production

To clarify the mechanisms by which the S198P mutation alters APP metabolism to enhance production of A $\beta$  peptides, we performed pulse-chase studies in APP695Swe no. 12 and APP695Swe/S198P no. 1 cells. Cells were pulse-labeled with L-[ $^{35}$ S]-methionine for 15 min and then chased for varying times in medium containing excess unlabeled L-methionine. The synthetic rates of full-length APP695Swe and APP695Swe/S198P were essentially identical (Fig. 2 A, lanes 1 and 2), and the rates of maturation of the immature APP695Swe and APP695Swe/S198P species were nearly indistinguishable (Fig. 2 A, lanes 3–12). Thus, the S198P mutation influences A $\beta$  production by a mechanism other than by altering the synthesis or maturation rate of immature APP. However, from the earliest time point of the chase (15 min) and onwards, the levels of both CTF $\alpha$  and CTF $\beta$ , generated by  $\alpha$ - and  $\beta$ -secretase cleavage of APP695, were elevated in the lysates of APP695Swe/S198P no. 1 cells, as were the levels of soluble APP (representing both sAPP695/S198PSwe $\alpha$  and sAPP695/S198PSwe $\beta$ ) in the CM (Fig. 2 A, lanes 4, 6, 8, 10, and 12) when compared with the levels of APP-CTFs and soluble APP695Swe in lysates and CM of the APPSwe no. 12 cell line, respectively (Fig. 2 A, lanes 3, 5, 7, 9, and 11). These findings would suggest that the presence of the S198P mutation somehow enhances egress of the chimeric APP from the ER to the Golgi, where BACE1 is active (Thinakaran et al., 1996), and to distal compartments where both BACE1 and  $\alpha$ -secretase are present. Finally, and confirming the MSD studies in Fig. 1, and consistent with the elevations in CTF $\alpha$  and CTF $\beta$  levels in lysates of APP695Swe/S198P no. 1 cells compared with APP695Swe no. 12 cells, steady-state labeling for 4 h revealed that the levels of radiolabeled A $\beta$  and p3, generated by  $\gamma$ -secretase processing of CTF $\beta$  and CTF $\alpha$ , respectively, were  $\sim 1.8\times$  higher in CM of APPSwe/S198P no. 1 cells compared with CM from APPSwe no. 12 cells (Fig. 2, B and C).

While the aforementioned studies would offer support for the model that introduction of the S198P mutation enhances egress of immature APPSwe/S198P, the pulse-labeling performed for 15 min does not just mark immature, asparagine-linked high

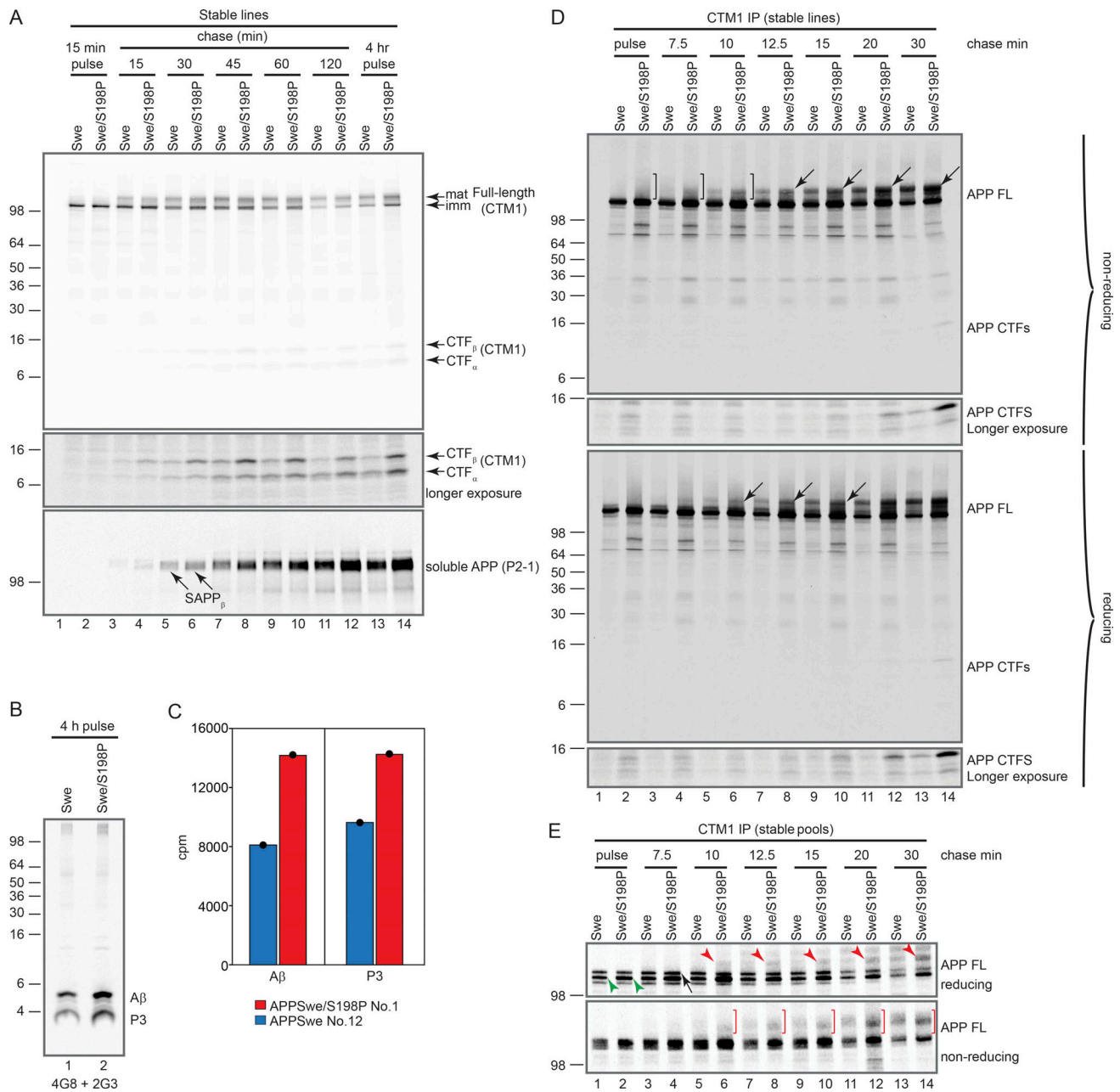


**Figure 2. Pulse-chase analysis of HEK293 cells stably expressing APP695Swe and APP695Swe/S198P. (A)** Pulse-chase analysis of HEK293 cell lines APPSwe no. 12 (Swe) and APPSwe/S198P no. 1 (Swe/S198P). Following pulse-labeling and chase or 4-h continuous labeling, APP metabolites immunoprecipitated with CTM1 antibody from cell lysates and with P2-1 antibody from CM were resolved on a Tris-Tricine gel (top and middle) and an SDS-PAGE (bottom), respectively. Black arrows indicate early secretion of SAPP<sub>β</sub> from APPSwe/S198P cells. **(B and C)** Immunoprecipitated Aβ and P3 from the CM of 4-h continuously labeled cells. **(D)** Pulse-chase analysis of HEK293 cell lines APP695Swe no. 12 (Swe) and APP695Swe/S198P no. 1 (Swe/S198P) with a 5-min pulse and chase. CTM1-immunoprecipitated (IP) APP metabolites from cell lysates were resolved on Tris-Tricine gels under both reducing and nonreducing conditions. In the nonreducing panel, the brackets mark heterogeneous, mature full-length APP that represents transient folding intermediates, and the black arrows indicate elevated mature APPSwe/S198P species; in the reducing panel, the black arrows indicate mature full-length APPSwe/S198P. **(E)** Pulse-chase analysis of HEK293 stable pools expressing APP695Swe (Swe) and APP695Swe/S198P (Swe/S198P) with a 5-min pulse and chase. CTM1-immunoprecipitated APP metabolites from cell lysates were resolved on Tris-Tricine gels under both reducing and nonreducing conditions. The red arrowheads represent mature, full-length APP695Swe/S198P in the presence of reducing reagent, while the red brackets represent heterogeneous species under nonreducing conditions that are present in APPSwe/S198P pools and represent transient folding intermediates. Green arrowheads indicate immature form of APP695Swe and APP695Swe/S198P, and the black arrow indicates the endogenous APP. imm, immature; mat, mature.

mannose APP species in the ER, but also a fraction of APP molecules that have exited to the Golgi, wherein trimming and subsequent conversion of high mannose oligosaccharides lead to the production of hybrid or complex-type oligosaccharides. The presence of both immature and mature full-length APP molecules during the pulse-labeling period supports this assertion (Fig. 2 A, lanes 1 and 2). With this concern, we repeated the study using a 5-min pulse-labeling period and shorter chase times to accurately capture synthesis and maturation of newly synthesized APPSwe and APPSwe/S198P. In addition, we followed a protocol by Jansens et al. (2002) that examined the folding of a multidomain protein, low-density lipoprotein receptor, which revealed that folding does not occur vectorially, but instead is mostly posttranslational and involves isomerization of transient long-range, nonnative disulfide bonds into short-range cysteine pairs. For APP, all 12 cysteine residues occur in the amino-terminal 187 amino acids (termed the “E1” domain; Fig. 1 A). Taking advantage of this fact, we immunoprecipitated full-length APP and APP-CTFs in lysates from the pulse-chase labeling study using CTM1 raised to the C-terminal 15 amino acids of APP (Vetrivel et al., 2009). The resulting immunoprecipitated material was split, and one half of the immunoprecipitate was boiled in Laemmli sample buffer (reducing), while the other half was boiled in Laemmli sample buffer lacking  $\beta$ -mercaptoethanol ( $\beta$ -ME; nonreducing). The underlying model is that when samples are denatured in the absence of reducing agent, a difference in SDS-PAGE mobility between nonreduced and the corresponding reduced samples indicates the presence of disulfide bonds. In our case, if folding of APPSwe/S198P occurs faster than APPSwe, we expected to observe transient folding intermediates at early time points under nonreducing conditions. Indeed, we now document that in nonreducing conditions (Fig. 2 D, top), the appearance of heterogeneous species that migrate with retarded mobility relative to immature APPSwe/S198P species in line no. 1 during the pulse-labeling period and during the first 10 min of the chase (bracket in Fig. 2 D, lanes 2, 4, and 6) compared with the pattern seen in APPSwe immunoprecipitates from line no. 12 (Fig. 2 D, lanes 1, 3, and 5). Moreover, the levels of mature APPSwe/S198P species in line no. 1 are clearly elevated at the 12.5-, 15-, 20-, and 30-min time points relative to the mature APPSwe species in line no. 12 (arrow, Fig. 2 D; compare lanes 8, 10, 12, and 14 to lanes 7, 9, 11, and 13), arguing for rapid maturation of the immature species. In denaturing conditions (Fig. 2 D, bottom), mature APPSwe/S198P molecules in line no. 1 appear earlier and at higher levels than APPSwe molecules in line no. 12 (Fig. 2 D; compare lanes 6, 8, and 10 to lanes 5, 7, and 9). Moreover, and consistent with the findings shown in Fig. 2 A, APP-CTFs are detected in lysates of APPSwe/S198P line no. 1 cells earlier (by 15 min; lane 10) and at higher levels in the chase than seen in APPSwe line no. 12 cells (Fig. 2 D, bottom; compare lanes 10, 12, and 14 to 9, 11, and 13).

One potential caveat of these latter studies is that we are comparing individual lines that may vary considerably with respect to their genetic content and regulation. To avoid these confounding issues, we prepared stable cell pools composed of between 50 and 100 independent colonies and repeated the pulse-chase experiments similar to that shown in Fig. 2 D. Pools

of HEK293 cells expressing either APPSwe or APPSwe/S198P were pulse-labeled with  $^{35}\text{S}$ -methionine for 5 min and chased in the presence of excess unlabeled L-methionine, as above. Analysis of CTM1 immunoprecipitates reveal essentially equivalent levels of newly synthesized APPSwe and APPSwe/S198P (Fig. 2 E, lanes 1, and 2) in both reducing (top) or nonreducing (bottom) conditions. Importantly, in nonreducing conditions, we detect heterogeneous species with reduced mobility beginning at 10 min into the chase period that is elevated in the APPSwe/S198P cell pool compared with the APPSwe cell pool (Fig. 2 E, bracket; compare lanes 6, 8, 10, and 12 with 5, 7, 9, and 11, respectively). These results, which in large part reflect the findings in Fig. 2 D, suggest the presence of transient folding intermediates in APPSwe/S198P cells at early time points after the pulse labeling. Moreover, in reducing conditions, we detect mature APPSwe/S198P in the cell pool with retarded mobility within 10 min of the chase compared with APPSwe in that pool (Fig. 2 E, top, red arrowhead; compare lanes 6, 8, 10, 12, and 14 with 5, 7, 9, 11, and 13, respectively). Hence, in both stable cell lines and in cell pools, APPSwe/S198P molecules are subject to accelerated folding and rapid maturation compared with APPSwe molecules.

While these latter studies lend support for the notion that the folding and maturation of APPSwe/S198P are more rapid than APPSwe, we felt it was critical to demonstrate this using a reagent that detects a folded domain within APP. To this end, we used monoclonal antibody P2-1, which recognizes an epitope(s) in the N-terminal domain of APP (Van Nostrand et al., 1989), a region that contains all 12 cysteine residues (Fig. 1 A). To establish the specificity of mAbP2-1, we treated detergent-solubilized extracts from APPSwe, APPSwe/S198P cells, and homogenates from brains of transgenic animals expressing APPSwe (ceAPPSwe/PS1 $\Delta$ E9) or APPSwe/S198P (APP695Swe/S198P/PS1 $\Delta$ E9; see below; Figs. 6, 7, and 8) with Laemmli buffer containing  $\beta$ -ME, or not, and performed Western blot analysis. MAbP2-1 failed to detect either APPSwe or APPSwe/S198P in cell or brain extracts that were treated with  $\beta$ -ME (Fig. 3 A, lanes 1–4, top), but readily detected APPSwe or APPSwe/S198P in cell extracts treated in the absence of  $\beta$ -ME (Fig. 3 A, lanes 5 and 6, top). Notably, mAbP2-1 failed to detect APPSwe or APPSwe/S198P in brain extracts (Fig. 3 A, lanes 7 and 8) because the APP transgene is a mouse APP695-human A $\beta$  chimera (see Materials and methods for details), thus confirming that this antibody is not only a sulfhydryl-dependent, conformation-specific antibody, but human APP-specific as well. As a control, we performed Western blots with mAb22C11, which detects a linear epitope between APP amino acids 66 and 81 that is identical between human and mouse APP (Hilbich et al., 1993). As expected, mAb22C11 readily detected APPSwe and APPSwe/S198P in both extracts from cultured cells or transgenic mouse brain, and independent of  $\beta$ -ME (Fig. 3 A, lanes 1–8, bottom).

To assess the utility of mAb P2-1 for our analysis, we first performed pulse chase/immunoprecipitation analysis on APPSwe no. 12 and APPSwe/S198P no. 1 cells. These studies revealed that while the structural epitope is readily detected in extracts from both cell lines that were pulse-labeled for 5 min (Fig. 3 B, lanes 1 and 8), the maturation of APPSwe/S198P

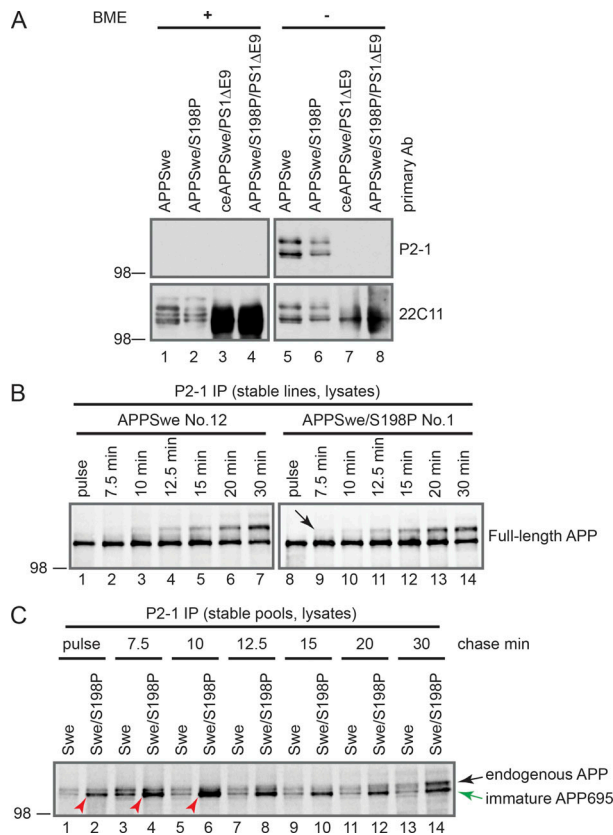


**Figure 3. Analysis of the metabolism of APPSwe and APPSwe/S198P with a sulfhydryl, confirmation-specific antibody, mAbP2-1. (A)** Validation of P2-1 antibody specificity in extracts from stably transfected cells and transgenic brain. Cell lysates of HEK293 cell pools stably expressing either APPSwe (lanes 1 and 5) or APPSwe/S198P (lanes 2 and 6), and brain lysates of transgenic mice expressing a chimeric mouse/human APPSwe (lanes 3 and 7) or APPSwe/S198P (lanes 4 and 8) were subject to reducing conditions with  $\beta$ -ME (lanes 1–4) or not (lanes 5–8) before electrophoresis. Upper two panels: P2-1 Western blots; lower two panels: 22C11 Western blots. P2-1 only recognizes nonreduced human APPSwe or APPSwe/S198P. **(B)** P2-1 immunoprecipitates (IP) from lysates of the stable cell lines APPSwe no. 12 (lanes 1–7) and APPSwe/S198P no. 1 (lanes 8–14) pulse-labeled for 5 min and chased. The black arrow in lane 9 indicates the early-appearing, correctly folded, and mature full-length APPSwe/S198P. **(C)** Pulse-chase analysis of HEK293 cell pools stably expressing APP695Swe (Swe) and APP695Swe/S198P (Swe/S198P) and immunoprecipitation with P2-1. Black arrow indicates endogenous immature APP; green arrow indicates immature APPSwe and APPSwe/S198P; red arrowheads indicate immature, folded full-length APP695Swe/S198P that appears early in the chase period. Ab, antibody; BME,  $\beta$ -mercaptoethanol.

occurred within 7.5 min compared with the first appearance of mature APPSwe at 10–12.5 min (Fig. 3 B, arrow, lane 9; compare with lane 2) and accumulated to higher levels (Fig. 3 B, compare lanes 10–14 with lanes 3–7). Extending this analysis, we assessed the appearance and maturation of the structural epitope detected by mAbP2-1 in stable cell pools expressing either APPSwe/S198P or APPSwe. We observed a clear difference in the rate of appearance, maturation, and levels of the mAbP2-1 epitope in extracts from cell pools expressing APPSwe/S198P compared with cell pools expressing APPSwe (Fig. 3 C, compare lanes 2, 4, 6, 8, 10, 12, and 14 with lanes 1, 3, 5, 7, 9, 11, and 13, respectively). Hence, our results are consistent with the view

that the generation and maturation of fully folded APPSwe/S198P occur more rapidly than APPSwe, which leads to an increase of secreted A $\beta$  in the CM.

### S198P mutation does not induce gross conformational changes in the APP ectodomain

The mechanism(s) by which the S198P mutation might influence the folding and rate of exit of APP695Swe/S198P from the ER are presently unclear, but the replacement of serine by a proline residue would likely introduce a “kink” in the structure and restrict protein flexibility, thus altering protein conformation that could, in turn, promote maturation and export. To examine this issue, we generated constructs containing cDNA encoding soluble forms of APP695 (sAPP695 $\alpha$ ) or APP965/S198P (sAPP695 $\alpha$ /S198P) with a C-terminal 6-His tag and then generated stable HEK293 cells that constitutively secrete these polypeptides. Secreted sAPP695 $\alpha$  or sAPP695 $\alpha$ /S198P molecules in the CM were purified to homogeneity by step-wise precipitation in 60% ammonium sulfate (Fig. 4 A), diethyl aminoethyl cellulose (DEAE) chromatography (Fig. 4 B), and elution from a Ni<sup>2+</sup> coupled to nitrilotriacetic acid (Ni-NTA) resin (Fig. 4 C). Isolated proteins were fractionated by SDS-PAGE, and silver staining verified the purity of sAPP695 $\alpha$  and sAPP695 $\alpha$ /S198P (Fig. 3 D). Circular dichroism (CD) spectroscopy (Johnson, 1990) revealed completely overlapping spectra indicating no gross differences in the secondary structures of the two proteins (Fig. 4 E). Furthermore, differential scanning fluorimetry (DSF; Simeonov, 2013), used to measure thermal stability, revealed that the presence of the S198P substitution did not significantly alter the  $\Delta T_m$  (change in melting temperature) of sAPP695 $\alpha$ /S198P relative to sAPP695 $\alpha$  (Fig. 4 F), a result that indirectly corroborates the CD studies. Thus, the presence of the S198P mutation had no impact on the secondary structure or thermal stability of sAPP695 $\alpha$ , arguing against the idea that gross conformational alterations induced the mutation.

### Generation and characterization of transgenic mice overexpressing APP695Swe/S198P

To extend the latter in vitro studies of APP metabolism (Figs. 1, 2, and 3) to an in vivo setting, the Cure Alzheimer’s Fund Genes-2-Therapy initiative generated transgenic mice that overexpressed mouse APP695 cDNA that contains the human A $\beta$  sequence together with the Swedish mutation (APP695Swe) or mouse APP695 cDNA together with the human A $\beta$  sequence, the Swedish mutation, and the S198P mutation (APP695Swe/S198P). The APP695Swe or APP695Swe/S198P transgenes are transcriptionally driven by the mouse prion protein (PrP) promoter (Borchelt et al., 1996a). Following pronuclear injections, we obtained three founder lines for each transgene. The expression of APP695Swe and APP695Swe/S198P in positive F1 animals was analyzed by Western blotting of brain lysates using human A $\beta$ -specific 6E10 antibody. Unfortunately, all three lines expressing APP695Swe expressed very low levels of the transgene-encoded polypeptide (Fig. 5 A). On the other hand, APP695Swe/S198P lines 15219 and 15222 (termed lines 19 and 22, respectively) showed high-level expression of the transgene, while line 15220 did not (Fig. 5 A, lanes 5–7, 6E10 panel). To examine the impact

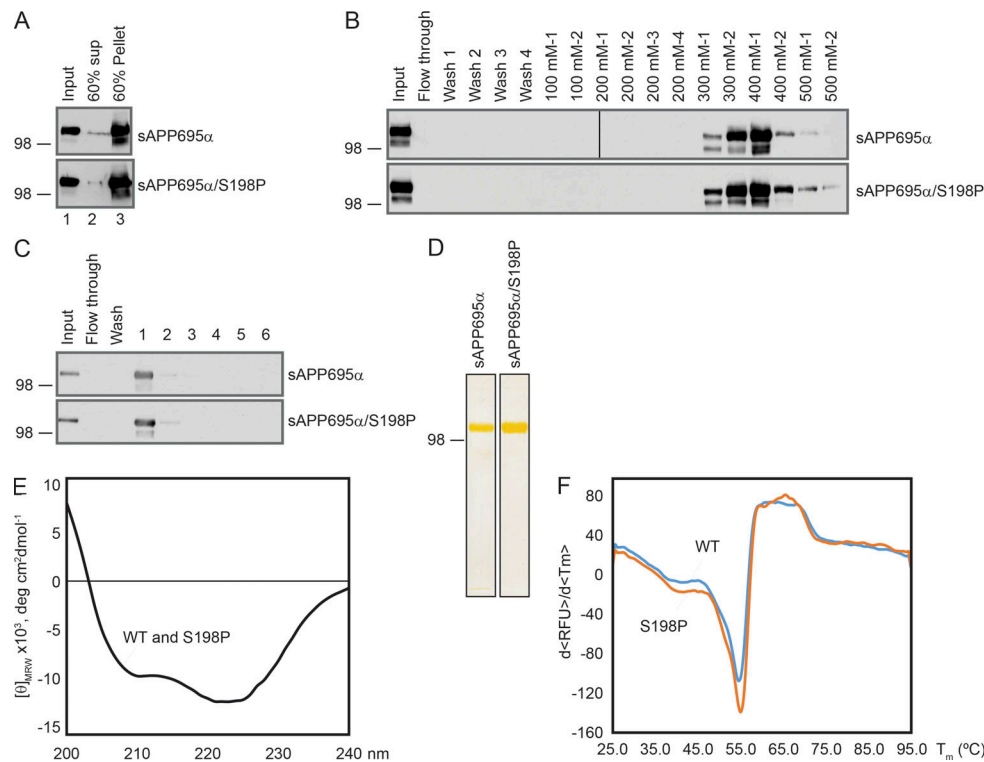


**Figure 4. Expression, purification, and CD spectroscopy, and DSF assays of sAPP695 $\alpha$  and sAPP695 $\alpha$ /S198P fragments.** (A) Ammonium sulfate fractionation of sAPP695 $\alpha$  and sAPP695 $\alpha$ /S198P fragments from CM. (B) Purification of soluble APP fragments by DEAE chromatography. (C) Purification of soluble APP fragments by Ni-NTA affinity resin. (D) Silver staining of purified soluble APP fragments. (E) CD spectra of purified sAPP695 $\alpha$  and sAPP695 $\alpha$ /S198P; the spectra of both purified fragments completely coincided. (F) DSF assay of purified sAPP695 $\alpha$  and sAPP695 $\alpha$ /S198P; both fragments showed the same thermostability. sup, supernatant.

of the APP695Swe/S198P on metabolism *in vivo*, and having failed to generate an APP695Swe line of comparable expression levels to APP695Swe/S198P lines 19 or 22, we chose to compare the expression of the APP695swe/S198P lines to APP695Swe levels in brain lysates of the ceAPPSwe/PS1 $\Delta$ E9 transgenic line, line 85, that harbors cointegrated transgenes encoding APP695Swe and PS1 $\Delta$ E9 that are transcriptionally driven by the mouse PrP promoter (Jankowsky et al., 2001). These studies revealed that APP695Swe expression in APP695Swe/S198P line 19 was comparable to the levels of APP695Swe in the ceAPPSwe/PS1 $\Delta$ E9 line and hence was selected for further analysis.

We previously demonstrated that PrP promoter-driven transgenic expression of APP695Swe to levels approximately twofold higher than endogenous APP (line C3-3) only begins to exhibit A $\beta$  deposition between the age of 18–20 mo (Borchelt et al., 1997). However, coexpression of the FAD-linked A246E PS1 (line N-5) or PS1 $\Delta$ E9 variants (line S-9) accelerates A $\beta$  deposition to 9 or 5–6 mo in brains of C3-3 mice (Borchelt et al., 1997; Lazarov et al., 2002), respectively. In view of these findings, we crossed APP695Swe/S198P line 19 mice to PrP promoter-driven PS1 $\Delta$ E9 transgenic line S-9 (Lee et al., 1997). To assess the impact of the transgenes on amyloid burden, it was critical to compare the levels of full-length APPSwe in age- and gender-matched ceAPPSwe/PS1 $\Delta$ E9 versus APP695Swe/S198P/PS1 $\Delta$ E9 mice. To specifically detect transgene-encoded APP and avoid detection of endogenous mouse APP, we employed mAb

6E10 (Kim et al., 1990) raised against amino acids 1–17 of human APP that is specific for human APP (Thinakaran et al., 1996); immunoselection of random sequences from a phage display library reveal that the minimum sequence required for mAb6E10 binding is R-x-D with the vast majority of these sequences containing an H at position x (R-H-D), corresponding to residues 5–7 of the A $\beta$  target sequence; human APP,.. R-H-D.. versus mouse,.. G-H-D.. (Baghallab et al., 2018). However, soluble sAPP $\alpha$  are also detected by mAb6E10, so we first immunoprecipitated full-length APP using APP C-terminal-specific antibodies, C1/6.1 or CTM1, then performed Western blot analysis of the resulting immunoprecipitates with mAb6E10 (Fig. 5 B). The intensity of full-length APP bands in Fig. 5 B revealed that the ratio of full-length, chimeric APP in the APP695Swe/S198P/PS1 $\Delta$ E9 line versus the ceAPPSwe/PS1 $\Delta$ E9 line is ~2:1 (Fig. 5 C) in 4-mo-old female, 6-mo-old male and female, and 9-mo-old male and female animals.

#### Elevated A $\beta$ peptides in brains of APPSwe/S198P/PS1 $\Delta$ E9 animals

Having demonstrated that A $\beta$  levels in the CM of HEK293 cells expressing APPSwe/S198P are significantly higher than those of cells expressing APPSwe, we examined A $\beta$  levels in brain lysates from PS1 $\Delta$ E9, APP695Swe/S198P, APP695Swe/S198P/PS1 $\Delta$ E9, and ceAPPSwe/PS1 $\Delta$ E9 animals. For every hemibrain, Tris-buffered saline (TBS)-soluble, detergent-soluble, and formic



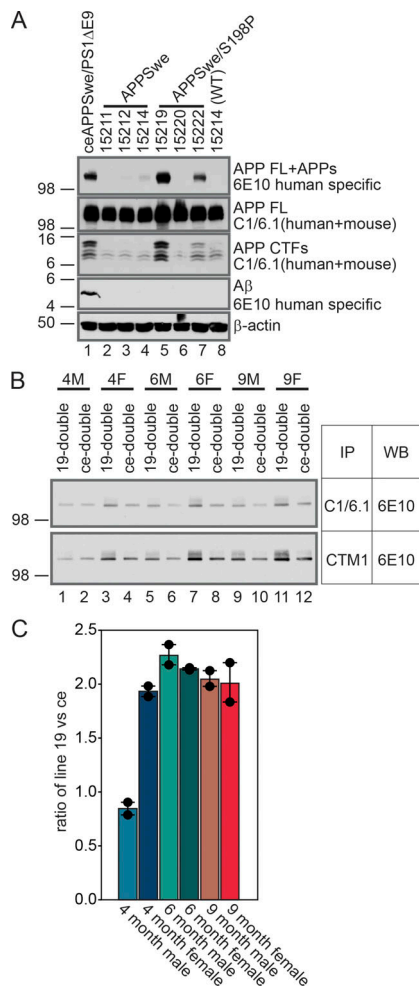


**Figure 5. Characterization of APP695Swe/S198P transgenic mice.** (A) Western blotting analysis of brain lysates from APP695Swe and APP695Swe/S198P transgenic lines. ceAPP695Swe/PS1ΔE9 was used as positive control, and nontransgenic littermate of line 15214 was used as negative control. Human APP-specific antibody 6E10 revealed high-level expression of APP695Swe/S198P in lines 15219 and 15222. (B and C) Immunoprecipitation (IP)–Western blotting (WB) analysis and density quantification with ImageJ software of the expression levels of APP695Swe/S198P (line 19) and APP695Swe in ceAPP695Swe/PS1ΔE9 transgenic mice. Both sets of immunoprecipitation–Western blotting were used for density quantification, and the results were represented by mean ± SEM, with the error bars representing SEM. F, female; M, male.

acid (FA)–soluble fractions were prepared and subject to Western blot analysis.

In 4-mo-old male and female animals, higher levels of soluble APP695 as well as α- and β-CTFs were observed in lysates from APP695Swe/S198P and APP695Swe/S198P/PS1ΔE9 animals compared with the levels in ceAPP695Swe/PS1ΔE9 animals (Fig. 6, A and B, APPSα and CTF panels), similar to the results observed in stably transfected HEK293 cells (Fig. 1, B and D). Similarly, the levels of TBS-soluble Aβ and detergent-soluble Aβ were detectable, albeit at low levels, in APP695Swe/S198P/PS1ΔE9 animals, but higher than the vanishingly low levels in ceAPP695Swe/PS1ΔE9 animals. MSD analysis confirmed these observations (Fig. 7 A). FA-soluble Aβ, representing Aβ species that are either deposited or aggregated as oligomers, was clearly elevated in APP695Swe/

S198P/PS1ΔE9 animals compared with the vanishing low levels seen in ceAPP695Swe/PS1ΔE9 animals and independent of gender at this time point (Fig. 6, A and B, FA-soluble panel; MSD quantified in Fig. 7 A). Notably, the levels of FA-soluble Aβ in female APP695Swe/S198P/PS1ΔE9 mice was significantly elevated compared with male mice, a finding consistent with earlier demonstrations that Aβ deposition in female ceAPP695Swe/PS1ΔE9 is accelerated relative to males (Lazarov et al., 2002; see Fig. 7, B–D, bottom).

In 6-mo-old animals, the levels of TBS-soluble Aβ, detergent-soluble Aβ, and FA-soluble Aβ were higher in APP695Swe/S198P/PS1ΔE9 animals compared with ceAPP695Swe/PS1ΔE9 animals and independent of gender (Fig. 6, C and D, all Aβ panels; MSD quantified in Fig. 7 A). The differences in FA-soluble Aβ levels between the mouse lines is consistent with the differences in Aβ burden assessed by immunohistochemistry (see Fig. 7, B–D, bottom).

In 9-mo-old animals, Aβ levels remained higher in the APP695Swe/S198P/PS1ΔE9 animals compared with the ceAPP695Swe/PS1ΔE9 animals, but the differences between groups were not as robust as in the 4-mo-old and 6-mo-old groups (Figs. 6 and 7).

#### Enhanced Aβ deposition in APP695Swe/S198P/PS1ΔE9 animals

Coronal sections of hemibrains of age- and gender-matched PS1ΔE9, APP695Swe/S198P, APP695Swe/S198P/PS1ΔE9, and ceAPP695Swe/PS1ΔE9 animals were subject to immunostaining with Aβ neo-epitope-specific 3D6 antibody (Bacskaï et al., 2001; Johnson-Wood et al., 1997; Kamenetz et al., 2003). As expected, no Aβ deposits were detectable in PS1ΔE9 animals at all ages, and deposits were also undetectable in sections from APP695Swe/S198P animals, independent of age and gender (Fig. 7 B). This was not unexpected as line C3-3 that expresses human APPSwe at approximately two times the level of endogenous APP, and at levels similar to human APPSwe in the APP695Swe/S198P line 19, does not exhibit Aβ deposition before 18 mo of age (Borchelt et al., 1997). On the other hand, Aβ deposition in sections from APP695Swe/S198P/PS1ΔE9 animals were significantly higher than age- and gender-matched ceAPP695Swe/PS1ΔE9 animals (Fig. 7 B; APP695Swe/S198P/PS1ΔE9 sections versus ceAPP695Swe/PS1ΔE9 sections; quantified in Fig. 7, C and D). Moreover, in 4-, 6-, and 9-mo-old female APP695Swe/S198P/PS1ΔE9 and ceAPP695Swe/PS1ΔE9 animals, we observed significantly higher levels of Aβ deposits compared with their male counterparts (Fig. 7 B; quantified in Fig. 7, C and D). It is also notable that the levels of FA-soluble Aβ40 and Aβ42 in APP695Swe/S198P/PS1ΔE9 and ceAPP695Swe/PS1ΔE9 animals, independent of gender, are very similar at 9 mo of age, thus suggesting that deposition has reached a plateau phase.

To determine the level of neuroinflammation and microglia, we costained brain sections from 4-, 6-, and 9-mo-old APP695Swe/S198P/PS1ΔE9 and ceAPP695Swe/PS1ΔE9 animals with 3D6 antibodies and Iba1 antibodies specific for ionized calcium binding adaptor molecule 1 (IBA-1), a microglia/macrophage-specific calcium-binding protein (Ahmed et al., 2007; Sasaki et al., 2001). We observed that independent of genotype, age,

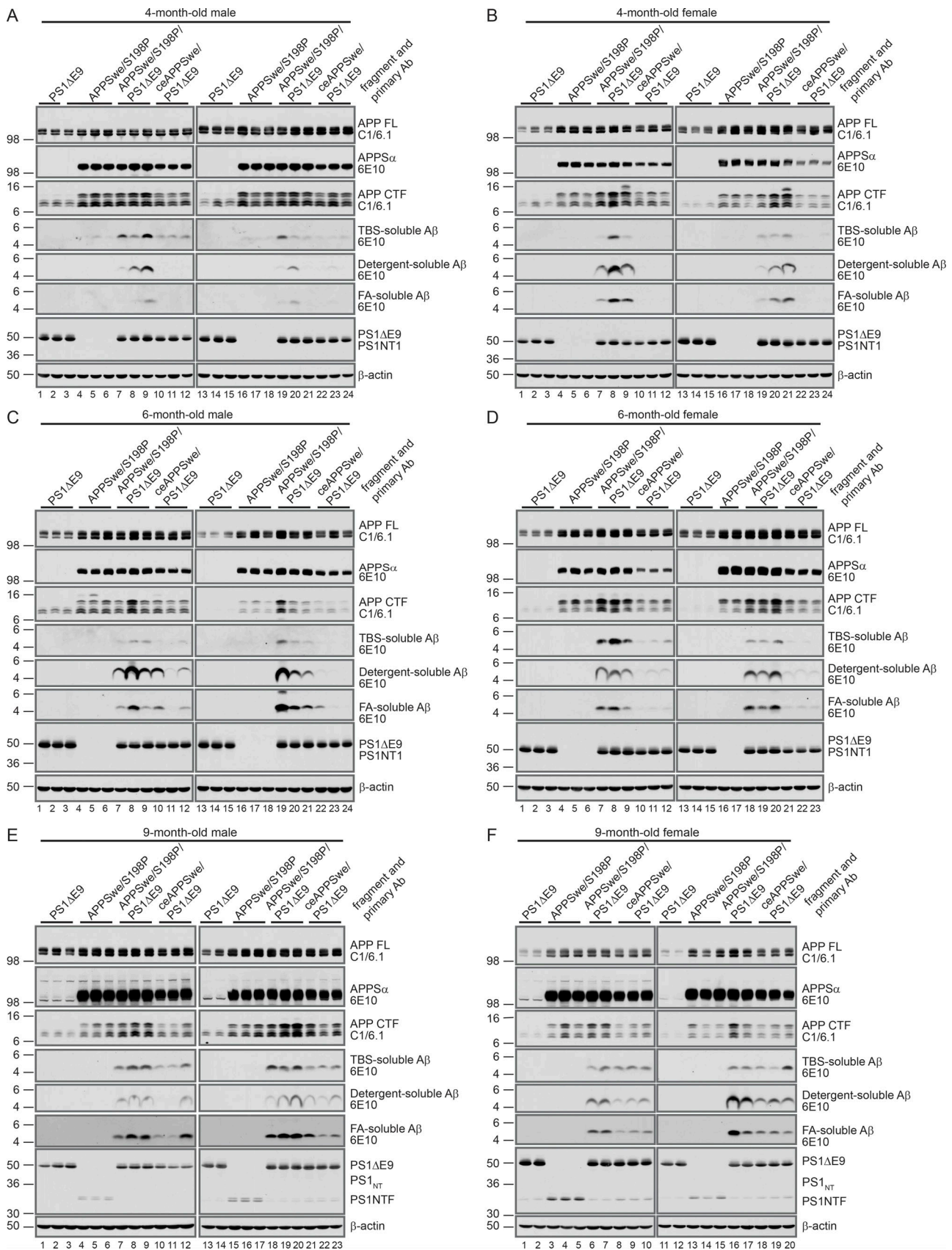


Figure 6. **Western blotting analysis of APP processing and A $\beta$  production in brain lysates of 4-mo-old, 6-mo-old, and 9-mo-old transgenic mice.** (A–F) TBS-soluble, detergent-soluble, and FA-soluble fractions of brain lysates were subject to Western blot analysis, PS1 $\Delta$ E9 animals were used as negative controls of exogenous APP expression, APP695Swe/S198P animals were used as negative controls of PS1 $\Delta$ E9 expression, and ceAPPSwe/PS1 $\Delta$ E9 animals were

used as positive controls of APP processing and A $\beta$  production. 4-mo-old animals (A and B), 6-mo-old animals (C and D), and 9-mo-old animals (E and F). Ab, antibody; FL, full-length.

or gender, all plaques were surrounded by Iba1-positive microglia (Fig. 8 A). We then sought to investigate the nature of plaques in the aforementioned groups of animals. Using Thioflavin S, a fluorescent probe that binds to dense-core A $\beta$  deposits in combination with 3D6 staining, we observe that all 3D6-positive plaques are thioflavin-positive. Finally, we costained sections from brains of the aforementioned cohorts with 3D6 and methoxy-X04, a derivative of Congo red and Chrysamine-G that has high in vitro binding affinity for A $\beta$  fibrils (dissociation constant [K<sub>i</sub>] = 26.8 nM) that is fluorescent and stains plaques, tangles, and cerebrovascular amyloid in postmortem sections of AD brain with good specificity (Klunk et al., 2002). Again, as we had observed with Thioflavin S costaining, all 3D6-positive plaques were costained with Methoxy-X04, arguing that the vast majority of, if not all, plaques in the brains of age- and gender-matched APP695Swe/S198P/PS1 $\Delta$ E9 and ceAPPSwe/PS1 $\Delta$ E9 animals are fibrillar in nature.

## Discussion

Rare, autosomal dominant FADs are caused by inheritance of mutations in genes encoding APP and presenilins. To date, all reported FAD-linked APP variants harbor missense mutations in exons 16 and 17 of the APP gene that encodes the A $\beta$  peptide (Fig. 1 A). Cell biological and biochemical approaches have been employed to establish the impact of each mutation on APP processing. For example, the Swedish KM-NL substitutions in exon 16 enhance cleavage by BACE1, thus generating elevated levels of APP-CTF $\beta$ , a substrate for  $\gamma$ -secretase processing that leads to elevated production of A $\beta$  peptides. On the other hand, APP variants with mutations within the transmembrane domain that are encoded in exon 17 lead to an elevation in the ratio of A $\beta$ 42 to A $\beta$ 40 peptides. In contrast to the reported FAD-linked APP mutations, the discovery of an extremely rare SNV in the WGS dataset from the NIMH AD family sample, now described as rs145081708, encoding a missense APP variant in exon 5 that corresponds to a Ser198Pro substitution, captured our attention. We now report on the impact of the S198P variant on APP metabolism and A $\beta$  production both in stably transfected mammalian cells and in transgenic mice and offer provocative insights pertaining to the mechanism by which this rare variant, albeit partially penetrant, drives A $\beta$  production and deposition in vivo.

First, we show that this rare variant was present in both affected siblings in one family with mixed early-late onset AD from the NIMH AD family sample. We also found this variant in an affected carrier and three unaffected carriers (age 72, 77, and 82 yr at last examination) who carried the APP-Ser198Pro mutation in the NIA ADSP cohorts. The unaffected subjects, together with the single unaffected monozygotic triplet in the Ashkenazi pedigree (Zhang et al., 2019a), would indicate this mutation is partially penetrant for AD risk. In addition, all AD patients identified in the present study who carried the

Ser198Pro mutation also carried an APOE- $\epsilon$ 4 allele, although one EOAD carrier was APOE- $\epsilon$ 2/ $\epsilon$ 4, a genotype considered to confer neutral risk for AD. However, the Ser198Pro mutation is too rare to carry out formal statistical analyses. These genetic findings together with the functional effects described herein would suggest that rs145081708 SNV that leads to the missense Ser198Pro substitution is a partially penetrant risk factor for AD that may be at least partially accounted for by interaction with the APOE- $\epsilon$ 4 allele. The identification of additional carriers of the Ser198Pro mutation will be necessary to get a better idea of this rare variant's effect size and penetrance for AD risk.

Second, we demonstrate that in stably transfected mammalian cells, expression of APP695Swe that also harbors the S198P mutation (APPSwe/S198P) leads to significantly elevated secretion of both A $\beta$ 40 and A $\beta$ 42 peptides compared with cells expressing APPSwe. Pulse-chase studies to assess the metabolism of APPSwe/S198P and APPSwe reveal that neither the synthesis nor the rate of maturation of immature APPSwe is altered by the S198P mutation. Comparison of the levels of soluble APPSwe/S198P and APPSwe in the CM from each cell line are instructive; we (Thinakaran et al., 1996) and others (Haass et al., 1995) have demonstrated that a significant fraction of APPSwe is subject to processing by BACE1 in Golgi and post-Golgi compartments, and we now observe that the levels of newly generated APPSwe/S198P $\beta$  detected in the CM of the APPSwe/S198P no. 1 cells are elevated at the earliest time points and all time points thereafter compared with the levels of sAPPSwe $\beta$  in the CM of APPSwe no. 12 cells (Fig. 2 A). Similarly, the levels of CTF $\beta$  are elevated in the lysates of APPSwe/S198P line no. 1 compared with the levels observed in lysates of the APPSwe line no. 12. Notably, and in contrast with the ~1:1 ratio of CTF $\alpha$ :CTF $\beta$  in the APPSwe line no. 12 at all time points up to 60 min, this ratio shifts to ~1:2 in the APPSwe/S198P line no. 1. We and others have shown that ~20–30% of newly synthesized APP in most mammalian cells arrives at the cell surface, and hence, a significant fraction of newly synthesized APPs are subject to ER-associated degradation and lysosomal degradation (Haass et al., 2012). Using short pulse-chase labeling paradigms and analysis of sulfhydryl-dependent transient folding intermediates, and immunoprecipitation with a sulfhydryl-dependent conformational antibody, we conclude that in contrast to APPSwe molecules, a fraction of APPSwe/S198P molecules that are normally subject to ER-associated degradation are insensitive to the ER degradation machinery because of enhanced folding and subsequent egress to the Golgi apparatus.

Third, and extending the findings in cultured cells, we document that coexpression of APP695Swe/S198P and PS1 $\Delta$ E9 in transgenic mice accelerates cerebral A $\beta$  deposition compared with animals that coexpress APP695Swe and PS1 $\Delta$ E9. The levels of A $\beta$  deposition observed in APP695Swe/S198P/PS1 $\Delta$ E9 are elevated at three different time points relative to the levels observed in APP695Swe/PS1 $\Delta$ E9 animals and independent of gender.

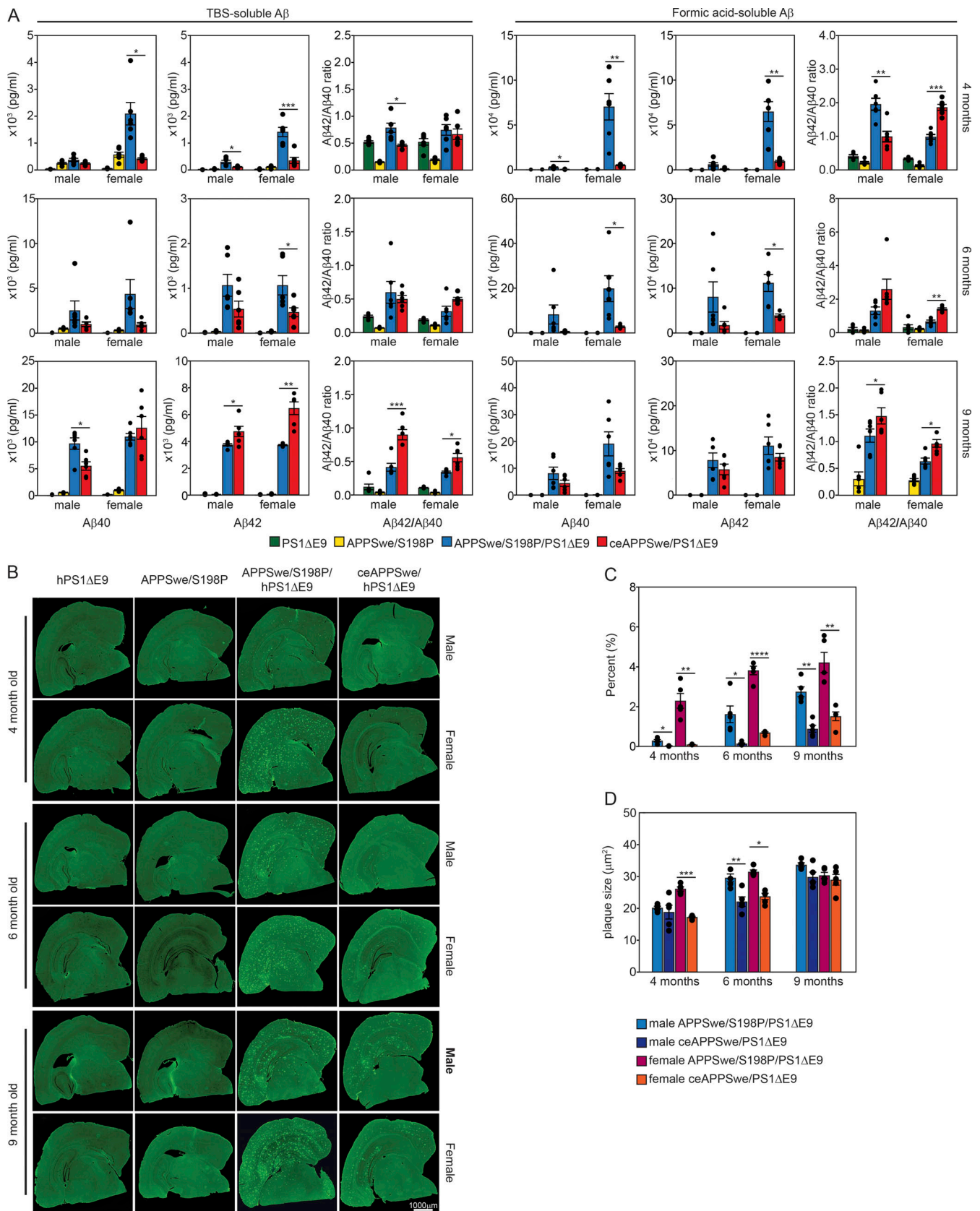


Figure 7. Quantification of TBS-soluble and FA-soluble A $\beta$  by MSD and amyloid burden analysis in the brains of 4-mo-old, 6-mo-old, and 9-mo-old PS1 $\Delta$ E9, APP695Swe/S198P, APP695Swe/S198P/PS1 $\Delta$ E9, and ceAPP695Swe/PS1 $\Delta$ E9 mice. (A) Quantification of TBS-soluble and FA-soluble A $\beta$  in the brain lysates of PS1 $\Delta$ E9, APP695Swe/S198P, APP695Swe/S198P/PS1 $\Delta$ E9, and ceAPP695Swe/PS1 $\Delta$ E9 mice. The levels of A $\beta$  were normalized to the expression levels of

full-length APP695Swe/S198P in APP695Swe/S198P/PS1ΔE9 mice and full-length APPSwe in ceAPPSwe/PS1ΔE9 mice. The results are represented by mean ± SEM, and the error bars represent SEM,  $n = 6$  animals. Two-way ANOVA with a two-stage linear step-up procedure of Benjamini, Krieger, and Yekutieli multiple comparisons post hoc tests was used to establish statistical significance. \*,  $P < 0.05$ ; \*\*,  $P < 0.01$ ; \*\*\*,  $P < 0.001$ . **(B)** Immunohistochemistry staining of amyloid plaques with Aβ 1–5-specific mAb3D6 in coronal brain sections of PS1ΔE9, APP695Swe/S198P, APP695Swe/S198P/PS1ΔE9, and ceAPPSwe/PS1ΔE9 mice. No amyloid plaques were detected on the sections of PS1ΔE9 and APP695Swe/S198P animals regardless of age (left two columns). Elevated level of amyloid plaques was detected on the sections of APP695Swe/S198P/PS1ΔE9 mice compared with that on the sections of age-matching ceAPPSwe/PS1ΔE9 mice. Scale bar, 1,000 μm. **(C)** Quantification of amyloid burden in APP695Swe/S198P/PS1ΔE9 and ceAPPSwe/PS1ΔE9 mice. Amyloid plaques on the brain sections of APP695Swe/S198P/PS1ΔE9 and ceAPPSwe/PS1ΔE9 animals stained with 3D6 were quantified with Fiji (ImageJ) software, and the results are represented by mean ± SEM, with the error bars representing SEM,  $n = 5$  animals. Two-way ANOVA with a two-stage linear step-up procedure of Benjamini, Krieger, and Yekutieli multiple comparisons post hoc tests was used to establish statistical significance. \*,  $P < 0.05$ ; \*\*,  $P < 0.01$ ; \*\*\*\*,  $P < 0.0001$ . **(D)** Analysis of plaque size on the sections stained with 3D6. The results are represented by mean ± SEM, with the error bars representing SEM,  $n = 5$  animals. Two-way ANOVA with a Tukey's multiple comparisons post hoc test was used to establish statistical significance. \*,  $P < 0.05$ ; \*\*,  $P < 0.01$ ; \*\*\*,  $P < 0.001$ .

The S198 residue is located in a highly flexible and extended acidic-rich domain (ala191-val290) that lies between two distinct structural domains of ~160 amino acids and ~190 amino acids in the APP695 ectodomain, termed the E1 and E2 domains, respectively (Coburger et al., 2013; Fig. 1 A). S198 has been shown to be a phosphorylation site in mammalian cells, but studies have shown that this modification only occurs in post-Golgi secretory vesicles or on the plasma membrane (Walter et al., 1997), and hence, the effects of the S198P mutation on processing of APPSwe/S198P at early times of the pulse-chase study cannot be explained by failed phosphorylation at amino acid 198. As S198 phosphosite-specific antibodies are unavailable, it is unclear whether this residue undergoes phosphorylation following biosynthesis. Alternatively, it is conceivable that the S198P mutation would affect N-linked oligosaccharide modifications at Asn467 and Asn467 (Pahlsson et al., 1992) or O-linked glycans at Thr291, Thr292, and Thr576 (Perdivara et al., 2009), and that these modifications might influence protein folding and intracellular transport or protein expression. Indeed, we do observe subtle differences in the levels of oligosaccharide modifications of APPSwe/S198P compared with APPSwe in the pulse-chase studies (Fig. 2, A, D, and E; and Fig. 3 B), and future biochemical studies will be necessary to identify the nature of these modifications. Regardless the outcomes of these studies, we do not implicate differences in processing and production of APPSwe/S198P metabolites as a function of protein conformation, as both our CD and DSF studies do not reveal any gross conformational alterations in the purified soluble ectodomain of APP695/S198P compared with the soluble ectodomain of APP695swe. Alternatively, it is plausible that conformational alterations occur within microdomains that would not be scored using our biophysical approaches.

We have demonstrated that cellular APP-CTFs and extracellular soluble APPSwe/S198P derived from the full-length APP S198P precursor appear at the earliest time points and accumulate to higher levels in pulse-chase experiments compared with the rate of production and accumulation of these metabolites derived from full-length APP695Swe. Moreover, our pulse-chase studies/immunoprecipitation studies suggest that transient folding intermediates occur in early points of the pulse-chase studies in cells expressing APPSwe/S198P compared with cells expressing APPSwe, a finding that argues for a more rapid folding of the S198P variant. In support of this observation, pulse-chase studies using the P2-1 antibody that is specific for a sulfhydryl-dependent

structural epitope in the amino-terminal E1 domain of APP reveal that folding of this domain occurs faster in cells expressing the APPSwe/S198P variant than in cells expressing APPSwe. In any event, and absent protein dynamic or crystallographic evidence for conformational alterations driven by the S198P mutation, we propose that the presence of the proline residue at position 198 enhances the rate of folding and exit of newly synthesized APPSwe/S198P from the ER to the Golgi and late compartments where BACE1 and  $\alpha$ -secretase are active.

How can the rate of folding of the APPSwe/S198P variant be accelerated relative to APPSwe? The determining factor is the introduction of proline, an amino acid that either breaks or kinks a helix, both because it cannot donate an amide hydrogen bond (having no amide hydrogen) and because its bulky pyrrolidine ring restricts the available conformational space. However, because proline is often seen as the first residue of a helix, it is presumed to be due to its structural rigidity. While prolines tend to be excluded from  $\alpha$ -helices and  $\beta$ -sheets, they can be situated at positions at the ends of these motifs. Thus, proline disrupts protein secondary structure by inhibiting the backbone to conform to an  $\alpha$ -helix or  $\beta$ -sheet conformation (Morgan and Rubenstein, 2013). An analysis of all proline residues and their local conformations extracted from the Brookhaven Protein Data Bank (MacArthur and Thornton, 1991) revealed that the residue preceding proline plays an important role in determining conformation. Interestingly, when proline follows an aspartate residue, there is a very high probability of the  $\alpha$  conformation being adopted ( $\alpha:\beta = 9:1$ ). In the case of APP695, the residue immediately preceding residue 198 is aspartate. In the absence of structural information, we offer a highly speculative model that the asp-pro pair promotes the generation of a local  $\alpha$ -helix that enhances the rate of folding of the surrounding E1 and E2 domains and the adjacent flexible domain. Our pulse-chase studies using the structural epitope-specific antibody mAbP2-1 provide support for this assertion (Fig. 3, B and C). Native cis-prolines have the largest effect on folding kinetics because the unfolded state favors trans-isomerization. In this regard, mutagenesis and folding studies of phosphoglycerate kinase (which contains a conserved cis-proline in position 204, in addition to several trans-prolines) revealed that fast folding events are sped up in the presence of the cis-proline, probably by restriction of the conformational space accessible to the molecule (Osváth and Gruebele, 2003).

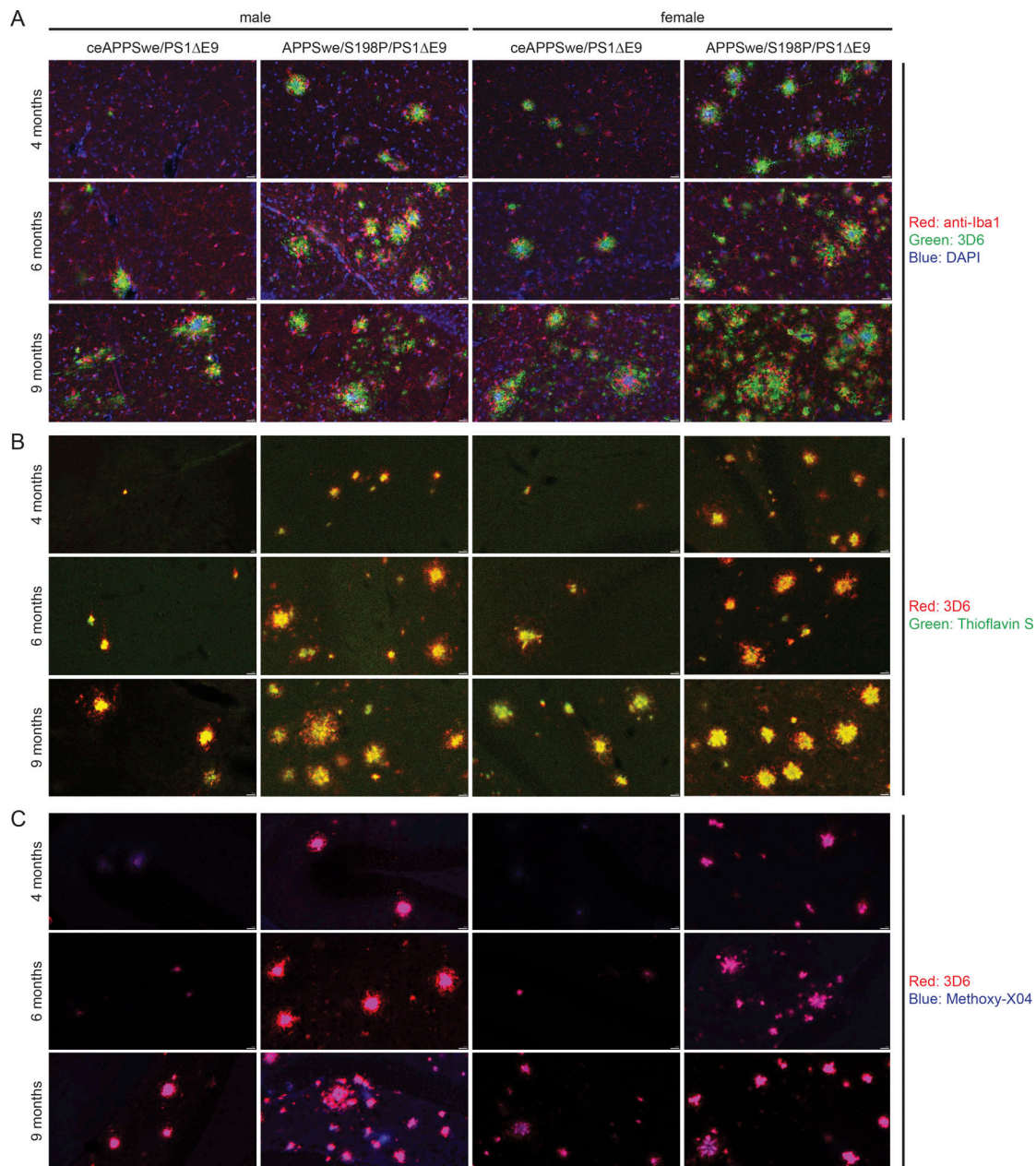


Figure 8. **Immunohistochemistry staining of brains sections of APP695Swe/S198P/PS1ΔE9 and ceAPP695Swe/PS1ΔE9 mice.** (A) Brain sections were costained with anti-Iba1 (red), 3D6 (green), and DAPI (blue). (B) Brain sections were costained with 3D6 (red) and Thioflavin S. (C) Brain sections were costained with 3D6 (red) and Methoxy-X04 (blue). Scale bar, 20 μm.

Our demonstration that the S198P mutation encoded by an SNV in exon 5 enhances Aβ production in mammalian cells and accelerates Aβ deposition in transgenic mice was surprising given the fact that all reported causative mutations in APP are found in exons 16 and 17, which also encode the Aβ domain. These findings beg the question of whether additional mutations that have been described in APP and found in individuals with EOAD might also have an impact on Aβ production. For example, the P620L mutation in exon 14 and K496Q mutation in exon 11 were identified in a British cohort composed of 47 unrelated EOAD cases and 179 elderly controls; AD cases were neuropathologically confirmed (Sassi et al., 2014). The authors claimed

that while they “cannot rule out a pathogenic role for APP K496Q and P620L, we suggest they are likely to be rare benign polymorphisms, as they cluster outside exon 16 and 17, where all pathogenic mutations have been reported up to date.” Similarly, additional APP variants (P299L, E296K, D243N, A235V, and P620A) were described in whole-exome sequencing in 424 French people with EOAD. The authors argued, “the significance of the APP rare variants—all located outside exons 16 and 17—remains to be determined, although their locations reasonably suffice to exclude a causative role in a Mendelian context” (Nicolas et al., 2016). Interestingly, we were unaware of any functional studies of the variants described by Sassi et al. (2014)

and Nicolas et al. (2016) with respect to A $\beta$  production, A $\beta$ 42/40 ratios, or fibrillogenesis of these peptides. However, and in view of the findings reported herein, and particularly with respect to mutations that replace proline residues that would impact structure of the macromolecule, we argue that cellular and transgenic approaches will be critical to determine the impact of novel, rare variants on A $\beta$  production and deposition before these are summarily dismissed as “benign” or “nonpathogenic” simply because the mutations reside outside of exons 16 and 17.

## Materials and methods

### cDNA constructs and cell lines

cDNA encoding either WT human APP695 (WT APP695) or the human APP Swedish KM-NL variant (APP695Swe) was subcloned into the pCB6 vector that contains sequences conferring resistance to neomycin, as described (Thinakaran et al., 1996). The S198P mutation was then engineered into the WT APP695 and APP695Swe cDNA constructs by PCR using primers S198P forward: 5'-ACAATGTGGATCCTGCTGATGCGGAG-3', and S198P reverse: 5'-CTCCGCATCAGCAGGATCCACATTGT-3'. The cDNAs encoding human sAPP695 $\alpha$  and sAPP695/S198P $\alpha$  were generated by PCR and cloned into pCB6 vector, and both constructs contained an extra 100-bp sequence upstream of the APP start codon to optimize translation efficiency. To generate transgenic mice overexpressing APP695Swe/S198P, we replaced sequences encoding the mouse A $\beta$  domain in mouse APP695 cDNA with sequences encoding the human A $\beta$  sequence and the Swedish mutations, as described earlier (Borchelt et al., 1996a). The S198P mutation was then introduced into this cDNA by PCR-based mutagenesis. This cDNA was then cloned into the unique XhoI site of a vector harboring the mouse prion promoter (MoPrP.Xho vector). All of the cDNA constructs were confirmed by DNA sequencing.

To analyze the expression and processing of WT APP695, WT APP695/S198P, APP695Swe, and APP695Swe/S198P, constructs encoding these polypeptides were expressed stably in HEK293 cells. For stable expression, the cDNA constructs were transfected into HEK293 cells using Lipofectamine 3000 reagent (Thermo Fisher Scientific), and cells with integrated cDNAs were selected with 400  $\mu$ g/ml Geneticin (G418; Life Technologies). The expression of these constructs in cell pools or in cell lines was confirmed by Western blot analysis.

### Generation of APP695Swe and APP695Swe/S198P transgenic mice

The MoPrP.Xho vector harboring APP695Swe or APP695Swe/S198P cDNA was digested with NotI (New England Biolabs), and the larger fragment was gel-purified (Gel Extraction Kit; Thermo Fisher Scientific) and eluted from the column with sterile TE injection buffer (5 mM Tris and 0.1 mM EDTA, pH 7.4). The concentration and the purity of the purified DNA fragments were determined by UV260 and the 260/280 ratio, respectively. For both APP695Swe and APP695Swe/S198P fragments, the concentration was adjusted to 20 ng/ $\mu$ l using sterile TE injection buffer, and the 260/280 ratio was  $\sim$ 1.9. The DNA was then injected into zygotes with a C57BL/6NTac background that were

transplanted into pseudo-pregnant recipient mice. Three lines each of APP695Swe and APP695Swe/S198P were identified by PCR using the following primers: PrP-sf: 5'-CCTCTTTGTGAC TATGTGGACTGATGTCGG-3', PrP-sr: 5'-GTGGATAACCCCTCC CCCAGCCTAGACC-3', and Fw3: 5'-ACGATGTCTTGGCCAACA TGATCAGTGAGC-3'. The PCR program used for genotyping was 94°C 1.5 min, 55°C 3 min, and 72°C 2 min for 35 cycles. To establish germline integration, founders was bred with C3H/Bl6 WT mice to generate F1 pups. Subsequently, the expression of APP695Swe or APP695Swe/S198P was examined by Western blot analysis using a human APP-specific antibody 6E10 (BioLegend). APP695Swe/S198P mice were then bred with mice expressing human presenilin 1  $\Delta$ E9 variant (PS1 $\Delta$ E9; line 9; Lee et al., 1997) to obtain mice that coexpress both APP695Swe/S198P and PS1 $\Delta$ E9 (APP695Swe/S198P/PS1 $\Delta$ E9 mice).

### Mouse handling and perfusions

The handling of experimental mice strictly followed the protocol approved by the Institutional Animal Care and Use Committee at the University of Chicago. Transgenic and WT control mice were anaesthetized with a mixture of ketamine and xylazine. The mice were then perfused with saline containing 1 mM EDTA for 4 min. Half of the brain was post-fixed in 4% paraformaldehyde for 24 h followed by dehydration in 30% sucrose, and the other half of the brain was immediately frozen on dry ice and stored in a  $-80^{\circ}$ C freezer before use.

### Immunohistochemistry

The hemibrains were sectioned on a microtome into 40-micron slices and stored in cryopreservation solution (25% glycerin and 30% ethylene glycol in 0.1 M phosphate buffer) at  $-20^{\circ}$ C before use. At least four sections from each animal were subject to mAb3D6 (Bacskaï et al., 2001; Johnson-Wood et al., 1997; Kamenetz et al., 2003) staining. The sections were washed six times for 10 min each in 1 $\times$  TBST buffer (TBS + 0.25% Triton X-100) followed by blocking for 2 h at room temperature in 5% donkey serum (Sigma-Aldrich). The sections were then incubated with 400 ng/ml of 3D6 antibody alone or together with the rabbit anti Iba1 antibody (cat. no. 019-19741; FUJIFILM Wako Pure Chemical Corporation; 1:500) in blocking solution overnight at 4°C. After six washes for 10 min each in 1 $\times$  TBST buffer, the sections were incubated with fluorescently conjugated secondary antibodies (cat. no. A21202, Invitrogen, anti-mouse Alexa 488, 1:500; cat. no. A32754, Invitrogen, anti-rabbit Alexa 594; or cat. no. A32742, Invitrogen, anti-mouse Alexa 594) in blocking solution for 1 h at room temperature, followed by three washes for 10 min each in TBST buffer. The sections were then incubated with DAPI (Invitrogen; 1:10,000) in TBS buffer for 5 min at room temperature and washed three times in TBS for 10 min each. The sections were mounted with FluoroMount (F4680-25ML; Sigma-Aldrich) and stored at 4°C overnight before scanning.

For costaining of sections by 3D6 and Thioflavin S (cat. no. T1892; Millipore Sigma), the immunostaining was performed as described above, and then free-floating sections were stained for 8 min with 0.002% Thioflavin S in 1 $\times$  TBS. The sections were rinsed in 50% ethanol twice for 1 min each, followed by a 5-min wash in 1 $\times$  TBS before mounting in FluoroMount.

For costaining of sections by 3D6 and Methoxy X04, the immunostaining was performed as above, and then free-floating sections were stained for 30 min with 50  $\mu$ M Methoxy-X04 (cat. no. 20476; Cayman Chemical) in TBS. The sections were washed three times with 1 $\times$  TBS before mounting in FluoroMount.

The slides for amyloid burden quantification were scanned using a 3DHistech Panoramic MIDI 20 $\times$  whole slide scanner, and the slides stained with 3D6, anti-Iba1, Thioflavin S, and Methoxy-X04 were scanned using a Caliber ID RS-G4 upright research confocal microscope. Scanned images were processed using CaseViewer (version 2.3) and Arivis Vision4D 3.3.

### Quantification of A $\beta$ burden

Coronal brain sections of APP695Swe/S198P/PS1 $\Delta$ E9 and ceAPPSwe/PS1 $\Delta$ E9 mice stained with 3D6 antibody were subjected to A $\beta$  burden analysis. At least four sections from each animal and five animals from each group (with same age, gender, and genotype) were used for the analysis. Total plaque numbers, the total area of A $\beta$  plaques in each section, and the percentage of area of each section occupied by A $\beta$  plaques were quantified with Fiji software (ImageJ 1.52p; National Institutes of Health) using methods described previously (Dodiya et al., 2019). Briefly, images captured under the same settings in CaseViewer were converted into 8-bit format and underwent binary conversion to have “fill holes” and “watershed” algorithms applied. A lower threshold limit of 50 and an upper threshold limit of 255 were applied to identify the plaques, and the amyloid burden was then calculated using the “analyze particles” plugin.

### Western blot and antibodies

For cultured HEK293 cells, the cells were lysed in a lysis buffer containing 50 mM Tris, pH 7.4, 150 mM NaCl, 5 mM EDTA, 0.5% NP-40, 0.5% sodium deoxycholate, 1 $\times$  protease inhibitor cocktail (Sigma-Aldrich), 1 mM PMSF (G Biosciences), and 1 $\times$  phosphatase inhibitor cocktails (Sigma-Aldrich). Cell lysates were quantified by bicinchoninic acid (BCA) protein assay kit (Pierce), and equal amounts of total proteins were fractionated on Tris-Tricine gels to analyze full-length APP and APP CTFs or on Tris-Glycine gels to analyze soluble APP. CM of the cultured cells was normalized to the concentration of cell lysates and was fractionated on Tris-Tricine gels to determine the level of A $\beta$ .

For the biochemical analysis of WT, APP695Swe/S198P, ceAPPSwe/PS1 $\Delta$ E9, and APP695Swe/S198P/PS1 $\Delta$ E9 brain samples, hemibrains were processed into three fractions as follows. The hemibrains were weighed and homogenized in 5 volumes of cold TBS buffer (50 mM Tris-Cl, pH 7.5, 150 mM NaCl, 5 mM EDTA, 1 $\times$  protease inhibitor cocktail, and 1 $\times$  phosphatase inhibitor) on ice for 20 strokes. The homogenate total TBS (TTBS) was divided into two parts: 500  $\mu$ l of the homogenate (TTBS1) was used to prepare TBS-soluble proteins, and the remaining homogenate (TTBS2, volume was measured) was saved for preparing detergent-soluble proteins. TTBS1 was subject to centrifugation at 100,000  $g$  for 1 h at 4°C. The supernatant fraction was saved as TBS-soluble proteins. The pellet fraction was extracted with 2.5 volumes of ice-cold 70% FA (based on the proportion of the original weight of the hemibrain used) by 20

pulses of sonication. The lysate was then subject to centrifugation at 100,000  $g$  for 1 h at 4°C, and the supernatant fraction was collected and represented FA-soluble proteins. To prepare detergent-soluble proteins, 0.25 volume of 5 $\times$  immunoprecipitation buffer (250 mM Tris-HCl, 750 mM NaCl, 5 mM EDTA, 2.5% NP-40, 2.5% sodium deoxycholate, 1 $\times$  protease inhibitor cocktail, and 1 $\times$  phosphatase inhibitor) was added to TTBS2. The sample was lysed on ice by 20 pulses of sonication, and was subject to centrifugation at 10,000  $g$  for 20 min at 4°C. The supernatant fraction represented total protein. Proteins in TBS-soluble and detergent-soluble fractions were quantified by the BCA protein assay kit (Pierce) and were used for the analysis of soluble APP, full-length APP, APP CTFs, TBS-soluble A $\beta$ , and detergent-soluble A $\beta$ . FA fractions were normalized to the TBS-soluble protein fraction before analysis.

To compare the expression levels of APP in ceAPPSwe/PS1 $\Delta$ E9 and APP695Swe/S198P/PS1 $\Delta$ E9 mice, detergent-soluble fractions of brain lysates were subject to immunoprecipitation with APP C-terminal antibodies, CTM1 (Vetrivel et al., 2009), or C1/6.1 (Biolegend), and the immunoprecipitated complexes were captured by protein A or protein G beads (Pierce) and released from the beads using Laemmli sample buffer and heating. The eluted proteins were resolved on a 10% SDS-PAGE, transferred to nitrocellulose membranes, and subjected to Western blot analysis with human-specific mAb6E10 (Kim et al., 1990) to detect overexpressed full-length APP.

For Western blot analysis, 6E10 was used to detect human full-length APP, soluble APP $\alpha$ , and A $\beta$ ; C1/6.1 (Biolegend) was used to detect full-length APP and APP CTFs; PS1<sub>NT</sub> (Zhang et al., 2020) and PS1 NT1 (Biolegend) were used to detect presenilin1. For pulse-chase experiments, P2-1 (Van Nostrand et al., 1989) was used to immunoprecipitate soluble APP, CTM1 was used to immunoprecipitate full-length APP and APP CTFs, and 4G8 (Zhang et al., 2014) and 2G3 (Johnson-Wood et al., 1997) were used to immunoprecipitate A $\beta$  and P3. Anti-6xHis (Genscript) was used to detect overexpressed and purified soluble APP $\alpha$ . Rabbit mAb GM130 (D6B1; cat. no. 12480S; Cell Signaling Technology) was used to detect the Golgi-resident protein GM130.

### Immunocytochemistry

HEK293 cells stably expressing APPSwe (line no. 12) or APPSwe/S198P (line no. 1) were seeded into a glass-bottom microwell dish (cat. P35G-1.5-14-C; MatTek). When cells reached the desired confluency, they were fixed in 4% paraformaldehyde and permeabilized in TBST for 10 min each at room temperature. After the cells were blocked in TBST containing 5% donkey serum for 1 h at room temperature, they were incubated with mAb3D6 and rabbit anti-GM130 antibody in blocking buffer at 4°C overnight. After the cells were washed three times with TBST at room temperature for 5 min each, they were incubated with appropriate secondary antibodies conjugated with Alexa 488 and Alexa 594 (Invitrogen) for 1 h at room temperature. Following three washes with TBST, the cells were stained with DAPI (Invitrogen; 1:10,000) for 5 min at room temperature and washed with TBS before images were taken using a Leica SP5 2-photon Laser Scanning Confocal system.



### MSD assays

The A $\beta$  levels were measured using the Meso Scale A $\beta$ -triplex 4G8 kits (Meso Scale Diagnostics LLC) as previously described (Minter et al., 2017). In brief, the 96-well plates were blocked with the diluents provided by the manufacturer with shaking for 1 h. Next the experimental samples and the protein standards were resuspended in the manufacturer-supplied detection antibodies. The mixed solutions were then placed on a shaker for 2 h, followed by washing and adding of the reading buffer. Electrochemiluminescence signals were captured by the Meso Scale SQ 120 system. A $\beta$  levels were determined by comparison to protein standards. For the detection of A $\beta$  levels in CM of cultured HEK293 cells, the CM collected from triplicated wells was analyzed individually. For the detection of A $\beta$  in brain samples, fractions of brain lysates from six animals in each group were analyzed.

### Pulse-chase experiments

HEK293 cells stably expressing APP695Swe or APP695Swe/S198P were seeded in 6-well plates the day before labeling so that the cells would be 75% confluent by the time of labeling. Before labeling, the medium was removed, and the cells were washed with methionine-free and serum-free DMEM (Invitrogen) twice. Methionine-free DMEM containing 1% dialyzed FCS (Invitrogen) was added to the plate, and the cells were incubated at 37°C for 1 h. 250  $\mu$ Ci of L-[<sup>35</sup>S]-methionine was then added to each well. For the chase experiment, the cells were labeled for 5 or 15 min at 37°C, the medium was collected, and the cells were washed once with PBS, and methionine-free DMEM containing 1% dialyzed FCS and 0.5 mM unlabeled L-methionine were added to each well. The cells were incubated at 37°C for a desired time period (for the 5-min pulse: 7.5, 10, 12.5, 15, 20, and 30 min; and for the 15-min pulse: 15, 30, 45, 60, and 120 min). At the end of each time point, the medium was collected, and the cells were washed once with PBS and lysed in cold immunoprecipitation buffer (150 mM NaCl, 50 mM Tris-Cl, pH 7.4, 0.5% NP-40, 0.5% sodium deoxycholate, 5 mM EDTA, and 1 $\times$  protease inhibitor cocktail). Cell lysates were cleared by centrifugation at 10,000 rpm in a microcentrifuge (Eppendorf) in a cold room, and the supernatant fraction was collected. For the detection of A $\beta$  and P3, the cells were continuously labeled with 250  $\mu$ Ci of L-[<sup>35</sup>S]-methionine for 4 h at 37°C. The specific activities of the lysates were determined using TCA precipitation and scintillation counting (LS6500; Beckman). The same amount of total cpm as the ones at 0 min was used for immunoprecipitation. Captured protein complexes were fractionated on Tris-Tricine or Tris-glycine gels and transferred to nitrocellulose blots, which were exposed to PhosphorImager Screens. The gel images were scanned using a Bio-Rad FX Pro Plus Molecular Imager or a Typhoon Trio Variable Mode Imager, and the counts of protein bands were quantified by the Quantity One software package or ImageQuant software.

### Purification of soluble sAPP695 $\alpha$ and soluble sAPP695 $\alpha$ /S198P fragments

CM of HEK293 cells stably expressing sAPP695 $\alpha$  or sAPP695 $\alpha$ /S198P was collected, and floating cells and other particulates

were removed by filtering the medium through a 0.45- $\mu$ m filter. The filtrate was supplemented with 1 mM PMSF and stored at -80°C before use. To purify soluble APP $\alpha$ , 540 ml of CM was thawed and allowed to reach room temperature, and 1.2 ml of 0.5 M EDTA, pH 8.0, and 60 ml of 1 M Tris-HCl, pH 8.0, were added to the CM. To concentrate soluble APP $\alpha$ , 233.90 g of ammonium sulfate was added to CM and stirred for 30 min at room temperature. The CM was subject to centrifugation at 6,000 rpm for 20 min at 20°C. The pellet was saved and dissolved in 9 ml of start buffer (25 mM Tris-HCl, pH 7.4, and 1 mM EDTA) and dialyzed against the start buffer overnight in a cold room. DEAE-Sepharose (Sigma-Aldrich) was equilibrated with the start buffer and degassed before it was used to pack a column. The dialyzed sample with a volume of 13.5 ml was loaded onto the DEAE column and eluted by step gradient using elution buffer (25 mM Tris-HCl, pH 7.4, 1 mM EDTA, and NaCl). The concentrations of NaCl used were 100 mM, 200 mM, 300 mM, 400 mM, and 500 mM. Peak fractions containing soluble APP were detected by Western blotting. The peak fractions eluted from the DEAE column (300 mM-2 and 400 mM-1) were pooled, concentrated, and dialyzed against a dialysis buffer (50 mM sodium phosphate, pH 7.4, 300 mM NaCl, and 10 mM imidazole), and its final volume was adjusted to 5 ml with the dialysis buffer. The sample was then mixed with 0.5 ml of preequilibrated Ni-NTA agarose beads (Invitrogen) and incubated in a cold room overnight. Captured protein was eluted with elution buffer (50 mM sodium phosphate, pH 7.4, 300 mM NaCl, and 300 mM imidazole). The protein peak was detected by Western blotting, and the purity of the protein was confirmed by silver staining.

### CD spectroscopy

Purified sAPP695 $\alpha$  and sAPP695 $\alpha$ /S198P were dialyzed against phosphate buffer (10 mM phosphate, pH 7.4, and 100 mM NaCl) at 4°C overnight. The concentrations of the sAPP695 $\alpha$  and sAPP695 $\alpha$ /S198P were determined by BCA assay and adjusted to 14.9  $\mu$ mol/liter. CD spectra for 180–260 nm in 1-nm steps with a 1-nm bandwidth were recorded at 25°C on a Jasco J-1500 CD Spectrometer using a 1-mm path-length quartz cuvette. Triplicate wavelength scans were averaged, buffer-subtracted, and converted to mean residual ellipticity as previously described.

### DSF

Purified sAPP695 $\alpha$  and sAPP695 $\alpha$ /S198P were dialyzed against phosphate buffer (50 mM phosphate, pH 7.4, and 150 mM NaCl) at 4°C overnight. The concentrations of sAPP695 $\alpha$  (390  $\mu$ g/ml) and sAPP695 $\alpha$ /S198P (560  $\mu$ g/ml) were determined by BCA assay. DSF measurements were performed on a CFX96 Real-Time System C1000 Thermal Cycler (Bio-Rad Laboratories). Each protein with a concentration of 1  $\mu$ M of was used in the reaction, and the commercial Sypro Orange solution (Invitrogen) was diluted 1,000-fold and used as 5 $\times$  stock. The reaction system contained 50 mM sodium phosphate buffer (pH 7.4), 150 mM sodium chloride, and 1 $\times$  Sypro Orange dye in a total volume of 25  $\mu$ l. Thermal melts were performed by heating the samples from 25°C to 95°C, increasing the temperature in steps of 0.5°C/30 s. Wavelengths of 490 and 575 nm were used for excitation

and emission, respectively. Samples were processed with the CFX software provided by the manufacturer.

### Statistical analysis

Statistical analysis was performed using GraphPad Prism software (GraphPad). One-way ANOVA with a Tukey's multiple-comparisons post hoc test was used for the analysis of the MSD measurement of A $\beta$  levels in the CM of the stable cell lines and stable cell pools expressing either APPSwe or APPSwe/S198P. Two-way ANOVA with a two-stage linear step-up procedure of Benjamini, Krieger, and Yekutieli multiple-comparisons post hoc tests was used for the analysis of the MSD measurements of soluble and insoluble A $\beta$  levels in the brain lysates of APPSwe/S198P/PS1 $\Delta$ E9 and ceAPPSwe/PS1 $\Delta$ E9 animals. Two-way ANOVA with a two-stage linear step-up procedure of Benjamini, Krieger, and Yekutieli multiple-comparisons post hoc tests was used for the analysis of amyloid burden, and two-way ANOVA with a Tukey's multiple-comparisons post hoc test was used for the analysis of plaque size in the brains of APPSwe/S198P/PS1 $\Delta$ E9 and ceAPPSwe/PS1 $\Delta$ E9 animals.

### Data availability

Relevant data are available from authors and/or included in the manuscript. The NIMH dataset analyzed during the current study is available from the corresponding author on reasonable request. The NIA ADSP WGS dataset is available from the Data Sharing Service National Institute of Aging Genetics of Alzheimer's Disease Data Storage Site under accession no. NG00067.

### Online supplemental material

Table S1 describes large WGS AD datasets.

### Acknowledgments

The authors would like to thank the staff from the NIMH and NIA for their help with this study. The authors thank Dr. Vytas Bindokas, Ms. Shirley Bond, and Dr. Christine Labno at the Microscopy Facility of the University of Chicago for their assistance with slide scanning and imaging, Dr. Elena Solomaha at the Biophysics Core Facility of the University of Chicago for assistance with CD assays, and Dr. Hemraj Dodiya for helpful information about Methoxy-XO4 staining. Finally, the authors thank Dr. Charles Barlowe, Chair and Professor of Biochemistry and Cell Biology at Dartmouth College Geisel School of Medicine, for invaluable advice on determination of folding and trafficking assays that were employed in this study.

This study is generously supported by the Cure Alzheimer's Fund (to S.S. Sisodia and R.E. Tanzi).

Author contributions: S.S. Sisodia and R.E. Tanzi initiated the project. S.S. Sisodia, R.E. Tanzi, and X. Zhang designed the overall study. X. Zhang generated APPSwe and APPSwe/S198P stable cell lines and transgenic mouse constructs and lines, performed pulse-chase labeling, Western blotting, immunohistochemistry, and immunocytochemistry staining, purified soluble APP fragments, performed CD spectra and DSF assays, analyzed experimental data, and prepared all figures and the manuscript. I.Q. Weigle performed amyloid burden quantification. W. Han

maintained the mouse colonies, performed genotyping, cut brain sections, and assisted with routine experiment preparations. M. Aryal generated APP695S198P and APP695Swe/S198P constructs and stable cell pools. D. Prokopenko carried out genetic analysis. Y. Liang carried out cell and animal-based MSD-A $\beta$  studies. S.Y. Zhen carried out animal-based MSD-A $\beta$  studies. C.M. Zhang analyzed and interpreted MSD-A $\beta$  findings. S.S. Sisodia and R.E. Tanzi critically analyzed all data and prepared the manuscript. All other coauthors edited the manuscript.

Disclosures: The authors declare no competing interests exist.

Submitted: 7 February 2021

Revised: 3 March 2021

Accepted: 3 March 2021

### References

- Ahmed, Z., G. Shaw, V.P. Sharma, C. Yang, E. McGowan, and D.W. Dickson. 2007. Actin-binding proteins coronin-1a and IBA-1 are effective microglial markers for immunohistochemistry. *J. Histochem. Cytochem.* 55: 687-700. <https://doi.org/10.1369/jhc.6A7156.2007>
- Bacskaï, B.J., S.T. Kajdasz, R.H. Christie, C. Carter, D. Games, P. Seubert, D. Schenk, and B.T. Hyman. 2001. Imaging of amyloid-beta deposits in brains of living mice permits direct observation of clearance of plaques with immunotherapy. *Nat. Med.* 7:369-372. <https://doi.org/10.1038/85525>
- Baghallab, I., J.M. Reyes-Ruiz, K. Abulnaja, E. Huwait, and C. Glabe. 2018. Epitomic Characterization of the Specificity of the Anti-Amyloid A $\beta$  Monoclonal Antibodies 6E10 and 4G8. *J. Alzheimers Dis.* 66:1235-1244. <https://doi.org/10.3233/JAD-180582>
- Beecham, G.W., J.C. Bis, E.R. Martin, S.H. Choi, A.L. DeStefano, C.M. van Duijn, M. Fornage, S.B. Gabriel, D.C. Kobooldt, D.E. Larson, et al. 2017. The Alzheimer's Disease Sequencing Project: Study design and sample selection. *Neurol. Genet.* 3:e194. <https://doi.org/10.1212/NXG.0000000000000194>
- Blackler, D., J.L. Haines, L. Rodes, H. Terwedow, R.C. Go, L.E. Harrell, R.T. Perry, S.S. Bassett, G. Chase, D. Meyers, et al. 1997. ApoE-4 and age at onset of Alzheimer's disease: the NIMH genetics initiative. *Neurology.* 48:139-147. <https://doi.org/10.1212/WNL.48.1.139>
- Borchelt, D.R., J. Davis, M. Fischer, M.K. Lee, H.H. Slunt, T. Ratovitsky, J. Regard, N.G. Copeland, N.A. Jenkins, S.S. Sisodia, and D.L. Price. 1996a. A vector for expressing foreign genes in the brains and hearts of transgenic mice. *Genet. Anal.* 13:159-163. [https://doi.org/10.1016/S1050-3862\(96\)00167-2](https://doi.org/10.1016/S1050-3862(96)00167-2)
- Borchelt, D.R., G. Thinakaran, C.B. Eckman, M.K. Lee, F. Davenport, T. Ratovitsky, C.M. Prada, G. Kim, S. Seekins, D. Yager, et al. 1996b. Familial Alzheimer's disease-linked presenilin 1 variants elevate Abeta1-42/1-40 ratio in vitro and in vivo. *Neuron.* 17:1005-1013. [https://doi.org/10.1016/S0896-6273\(00\)80230-5](https://doi.org/10.1016/S0896-6273(00)80230-5)
- Borchelt, D.R., T. Ratovitsky, J. van Lare, M.K. Lee, V. Gonzales, N.A. Jenkins, N.G. Copeland, D.L. Price, and S.S. Sisodia. 1997. Accelerated amyloid deposition in the brains of transgenic mice coexpressing mutant presenilin 1 and amyloid precursor proteins. *Neuron.* 19:939-945. [https://doi.org/10.1016/S0896-6273\(00\)80974-5](https://doi.org/10.1016/S0896-6273(00)80974-5)
- Citron, M., T. Oltersdorf, C. Haass, L. McConlogue, A.Y. Hung, P. Seubert, C. Vigo-Pelfrey, I. Lieberburg, and D.J. Selkoe. 1992. Mutation of the beta-amyloid precursor protein in familial Alzheimer's disease increases beta-protein production. *Nature.* 360:672-674. <https://doi.org/10.1038/360672a0>
- Coburger, I., S.O. Dahms, D. Roeser, K.H. Gührs, P. Hortschansky, and M.E. Than. 2013. Analysis of the overall structure of the multi-domain amyloid precursor protein (APP). *PLoS One.* 8:e81926. <https://doi.org/10.1371/journal.pone.0081926>
- De Jonghe, C., C. Esselens, S. Kumar-Singh, K. Craessaerts, S. Serneels, F. Checler, W. Annaert, C. Van Broeckhoven, and B. De Strooper. 2001. Pathogenic APP mutations near the gamma-secretase cleavage site differentially affect Abeta secretion and APP C-terminal fragment stability. *Hum. Mol. Genet.* 10:1665-1671. <https://doi.org/10.1093/hmg/10.16.1665>
- De Strooper, B. 2007. Loss-of-function presenilin mutations in Alzheimer disease. Talking Point on the role of presenilin mutations in Alzheimer

- disease. *EMBO Rep.* 8:141–146. <https://doi.org/10.1038/sj.embor.7400897>
- De Strooper, B., and W. Annaert. 2000. Proteolytic processing and cell biological functions of the amyloid precursor protein. *J. Cell Sci.* 113: 1857–1870.
- Dodiya, H.B., T. Kuntz, S.M. Shaik, C. Baufeld, J. Leibowitz, X. Zhang, N. Gattel, X. Zhang, O. Butovsky, J.A. Gilbert, and S.S. Sisodia. 2019. Sex-specific effects of microbiome perturbations on cerebral A $\beta$  amyloidosis and microglia phenotypes. *J. Exp. Med.* 216:1542–1560. <https://doi.org/10.1084/jem.20182386>
- Glennner, G.G., and C.W. Wong. 1984. Alzheimer's disease: initial report of the purification and characterization of a novel cerebrovascular amyloid protein. *Biochem. Biophys. Res. Commun.* 120:885–890. [https://doi.org/10.1016/S0006-291X\(84\)80190-4](https://doi.org/10.1016/S0006-291X(84)80190-4)
- Haass, C., C.A. Lemere, A. Capell, M. Citron, P. Seubert, D. Schenk, L. Lannfelt, and D.J. Selkoe. 1995. The Swedish mutation causes early-onset Alzheimer's disease by beta-secretase cleavage within the secretory pathway. *Nat. Med.* 1:1291–1296. <https://doi.org/10.1038/nm1295-1291>
- Haass, C., C. Kaether, G. Thinakaran, and S. Sisodia. 2012. Trafficking and proteolytic processing of APP. *Cold Spring Harb. Perspect. Med.* 2: a006270. <https://doi.org/10.1101/cshperspect.a006270>
- Hardy, J., and D. Allsop. 1991. Amyloid deposition as the central event in the aetiology of Alzheimer's disease. *Trends Pharmacol. Sci.* 12:383–388. [https://doi.org/10.1016/0165-6147\(91\)90609-V](https://doi.org/10.1016/0165-6147(91)90609-V)
- Hilbich, C., U. Mönning, C. Grund, C.L. Masters, and K. Beyreuther. 1993. Amyloid-like properties of peptides flanking the epitope of amyloid precursor protein-specific monoclonal antibody 22C11. *J. Biol. Chem.* 268:26571–26577. [https://doi.org/10.1016/S0021-9258\(19\)74350-6](https://doi.org/10.1016/S0021-9258(19)74350-6)
- Hunter, S., and C. Brayne. 2018. Understanding the roles of mutations in the amyloid precursor protein in Alzheimer disease. *Mol. Psychiatry.* 23: 81–93. <https://doi.org/10.1038/mp.2017.218>
- Jankowsky, J.L., H.H. Slunt, T. Ratovitski, N.A. Jenkins, N.G. Copeland, and D.R. Borchelt. 2001. Co-expression of multiple transgenes in mouse CNS: a comparison of strategies. *Biomol. Eng.* 17:157–165. [https://doi.org/10.1016/S1389-0344\(01\)00067-3](https://doi.org/10.1016/S1389-0344(01)00067-3)
- Jankowsky, J.L., D.J. Fadale, J. Anderson, G.M. Xu, V. Gonzales, N.A. Jenkins, N.G. Copeland, M.K. Lee, L.H. Younkin, S.L. Wagner, et al. 2004. Mutant presenilins specifically elevate the levels of the 42 residue beta-amyloid peptide in vivo: evidence for augmentation of a 42-specific gamma secretase. *Hum. Mol. Genet.* 13:159–170. <https://doi.org/10.1093/hmg/ddh019>
- Jansens, A., E. van Duijn, and I. Braakman. 2002. Coordinated nonvectorial folding in a newly synthesized multidomain protein. *Science.* 298: 2401–2403. <https://doi.org/10.1126/science.1078376>
- Johnson, W.C. Jr. 1990. Protein secondary structure and circular dichroism: a practical guide. *Proteins.* 7:205–214. <https://doi.org/10.1002/prot.340070302>
- Johnson-Wood, K., M. Lee, R. Motter, K. Hu, G. Gordon, R. Barbour, K. Khan, M. Gordon, H. Tan, D. Games, et al. 1997. Amyloid precursor protein processing and A beta42 deposition in a transgenic mouse model of Alzheimer disease. *Proc. Natl. Acad. Sci. USA.* 94:1550–1555. <https://doi.org/10.1073/pnas.94.4.1550>
- Kamenetz, F., T. Tomita, H. Hsieh, G. Seabrook, D. Borchelt, T. Iwatsubo, S. Sisodia, and R. Malinow. 2003. APP processing and synaptic function. *Neuron.* 37:925–937. [https://doi.org/10.1016/S0896-6273\(03\)00124-7](https://doi.org/10.1016/S0896-6273(03)00124-7)
- Kim, K., G. Wen, C. Bancher, C. Chen, V. Sapienza, H. Hong, and H. Wisniewski. 1990. Detection and quantitation of amyloid beta-peptide with 2 monoclonal antibodies. *Neurosci. Res. Commun.* 7:113–122.
- Kim, S.H., J.Y. Leem, J.J. Lah, H.H. Slunt, A.I. Levey, G. Thinakaran, and S.S. Sisodia. 2001. Multiple effects of aspartate mutant presenilin 1 on the processing and trafficking of amyloid precursor protein. *J. Biol. Chem.* 276:43343–43350. <https://doi.org/10.1074/jbc.M108245200>
- Klunk, W.E., B.J. Bacskai, C.A. Mathis, S.T. Kajdasz, M.E. McLellan, M.P. Froesch, M.L. Debnath, D.P. Holt, Y. Cheng, and B.T. Hyman. 2002. Imaging A beta plaques in living transgenic mice with multiphoton microscopy and methoxy-XO4, a systemically administered Congo red derivative. *J. Neuropathol. Exp. Neurol.* 61:797–805. <https://doi.org/10.1093/jnen/61.9.797>
- Kumar-Singh, S., C. De Jonghe, M. Cruts, R. Kleinert, R. Wang, M. Mercken, B. De Strooper, H. Vanderstichele, A. Löfgren, I. Vanderhoeven, et al. 2000. Nonfibrillar diffuse amyloid deposition due to a gamma(42)-secretase site mutation points to an essential role for N-truncated A beta(42) in Alzheimer's disease. *Hum. Mol. Genet.* 9:2589–2598. <https://doi.org/10.1093/hmg/9.18.2589>
- Landrum, M.J., J.M. Lee, M. Benson, G.R. Brown, C. Chao, S. Chitipiralla, B. Gu, J. Hart, D. Hoffman, W. Jang, et al. 2018. ClinVar: improving access to variant interpretations and supporting evidence. *Nucleic Acids Res.* 46(D1):D1062–D1067. <https://doi.org/10.1093/nar/gkx1153>
- Lazarov, O., M. Lee, D.A. Peterson, and S.S. Sisodia. 2002. Evidence that synaptically released beta-amyloid accumulates as extracellular deposits in the hippocampus of transgenic mice. *J. Neurosci.* 22:9785–9793. <https://doi.org/10.1523/JNEUROSCI.22-22-09785.2002>
- Lee, M.K., D.R. Borchelt, G. Kim, G. Thinakaran, H.H. Slunt, T. Ratovitski, L.J. Martin, A. Kittur, S. Gandy, A.I. Levey, et al. 1997. Hyperaccumulation of FAD-linked presenilin 1 variants in vivo. *Nat. Med.* 3:756–760. <https://doi.org/10.1038/nm0797-756>
- MacArthur, M.W., and J.M. Thornton. 1991. Influence of proline residues on protein conformation. *J. Mol. Biol.* 218:397–412. [https://doi.org/10.1016/0022-2836\(91\)90721-H](https://doi.org/10.1016/0022-2836(91)90721-H)
- Masters, C.L., G. Simms, N.A. Weinman, G. Multhaup, B.L. McDonald, and K. Beyreuther. 1985. Amyloid plaque core protein in Alzheimer disease and Down syndrome. *Proc. Natl. Acad. Sci. USA.* 82:4245–4249. <https://doi.org/10.1073/pnas.82.12.4245>
- Minter, M.R., R. Hinterleitner, M. Meisel, C. Zhang, V. Leone, X. Zhang, P. Oyler-Castrillo, X. Zhang, M.W. Musch, X. Shen, et al. 2017. Antibiotic-induced perturbations in microbial diversity during post-natal development alters amyloid pathology in an aged APP<sup>SWE</sup>/PS1<sup>ΔE9</sup> murine model of Alzheimer's disease. *Sci. Rep.* 7:10411. <https://doi.org/10.1038/s41598-017-11047-w>
- Morgan, A.A., and E. Rubenstein. 2013. Proline: the distribution, frequency, positioning, and common functional roles of proline and polyproline sequences in the human proteome. *PLoS One.* 8:e53785. <https://doi.org/10.1371/journal.pone.0053785>
- Nicolas, G., D. Wallon, C. Charbonnier, O. Quenez, S. Rousseau, A.C. Richard, A. Rovelet-Lecrux, S. Coutant, K. Le Guennec, D. Bacq, et al. 2016. Screening of dementia genes by whole-exome sequencing in early-onset Alzheimer disease: input and lessons. *Eur. J. Hum. Genet.* 24: 710–716. <https://doi.org/10.1038/ejhg.2015.173>
- Osváth, S., and M. Gruebele. 2003. Proline can have opposite effects on fast and slow protein folding phases. *Biophys. J.* 85:1215–1222. [https://doi.org/10.1016/S0006-3495\(03\)74557-3](https://doi.org/10.1016/S0006-3495(03)74557-3)
- Pahlsson, P., S.H. Shakin-Eshleman, and S.L. Spitalnik. 1992. N-linked glycosylation of beta-amyloid precursor protein. *Biochem. Biophys. Res. Commun.* 189:1667–1673. [https://doi.org/10.1016/0006-291X\(92\)90269-Q](https://doi.org/10.1016/0006-291X(92)90269-Q)
- Perdivara, I., R. Petrovich, B. Allinquant, L.J. Detering, K.B. Tomer, and M. Przybylski. 2009. Elucidation of O-glycosylation structures of the beta-amyloid precursor protein by liquid chromatography-mass spectrometry using electron transfer dissociation and collision induced dissociation. *J. Proteome Res.* 8:631–642. <https://doi.org/10.1021/pr800758g>
- Price, D.L., R.E. Tanzi, D.R. Borchelt, and S.S. Sisodia. 1998. Alzheimer's disease: genetic studies and transgenic models. *Annu. Rev. Genet.* 32: 461–493. <https://doi.org/10.1146/annurev.genet.32.1.461>
- Prokopenko, D., J. Hecker, R. Kirchner, B.A. Chapman, O. Hoffman, K. Mullin, W. Hide, L. Bertram, N. Laird, D.L. DeMeo, et al. 2020. Identification of Novel Alzheimer's Disease Loci Using Sex-Specific Family-Based Association Analysis of Whole-Genome Sequence Data. *Sci. Rep.* 10:5029. <https://doi.org/10.1038/s41598-020-61883-6>
- Sasaki, Y., K. Ohsawa, H. Kanazawa, S. Kohsaka, and Y. Imai. 2001. Ibal is an actin-cross-linking protein in macrophages/microglia. *Biochem. Biophys. Res. Commun.* 286:292–297. <https://doi.org/10.1006/bbrc.2001.5388>
- Sassi, C., R. Guerreiro, R. Gibbs, J. Ding, M.K. Lupton, C. Troakes, K. Lunnon, S. Al-Sarraj, K.S. Brown, C. Medway, et al. ARUK Consortium. 2014. Exome sequencing identifies 2 novel presenilin 1 mutations (p.L166V and p.S230R) in British early-onset Alzheimer's disease. *Neurobiol. Aging.* 35:2422.e13–2422.e16. <https://doi.org/10.1016/j.neurobiolaging.2014.04.026>
- Simeonov, A. 2013. Recent developments in the use of differential scanning fluorometry in protein and small molecule discovery and characterization. *Expert Opin. Drug Discov.* 8:1071–1082. <https://doi.org/10.1517/17460441.2013.806479>
- Thinakaran, G., D.B. Teplow, R. Siman, B. Greenberg, and S.S. Sisodia. 1996. Metabolism of the "Swedish" amyloid precursor protein variant in neuro2a (N2a) cells. Evidence that cleavage at the "beta-secretase" site occurs in the golgi apparatus. *J. Biol. Chem.* 271:9390–9397. <https://doi.org/10.1074/jbc.271.16.9390>
- Van Broeckhoven, C., and S. Kumar-Singh. 2006. Genetics and pathology of alpha-secretase site AbetaPP mutations in the understanding of Alzheimer's disease. *J. Alzheimers Dis.* 9(3, Suppl):389–398. <https://doi.org/10.3233/JAD-2006-9S344>
- Van Nostrand, W.E., S.L. Wagner, M. Suzuki, B.H. Choi, J.S. Farrow, J.W. Geddes, C.W. Cotman, and D.D. Cunningham. 1989. Protease nexin-II, a

- potent antichymotrypsin, shows identity to amyloid beta-protein precursor. *Nature*. 341:546–549. <https://doi.org/10.1038/341546a0>
- Vassar, R., B.D. Bennett, S. Babu-Khan, S. Kahn, E.A. Mendiaz, P. Denis, D.B. Teplow, S. Ross, P. Amarante, R. Loeloff, et al. 1999. Beta-secretase cleavage of Alzheimer's amyloid precursor protein by the transmembrane aspartic protease BACE. *Science*. 286:735–741. <https://doi.org/10.1126/science.286.5440.735>
- Vetrivel, K.S., X. Meckler, Y. Chen, P.D. Nguyen, N.G. Seidah, R. Vassar, P.C. Wong, M. Fukata, M.Z. Kounnas, and G. Thinakaran. 2009. Alzheimer disease A $\beta$  production in the absence of S-palmitoylation-dependent targeting of BACE1 to lipid rafts. *J. Biol. Chem.* 284:3793–3803. <https://doi.org/10.1074/jbc.M808920200>
- Walter, J., A. Capell, A.Y. Hung, H. Langen, M. Schnölzer, G. Thinakaran, S.S. Sisodia, D.J. Selkoe, and C. Haass. 1997. Ectodomain phosphorylation of beta-amyloid precursor protein at two distinct cellular locations. *J. Biol. Chem.* 272:1896–1903. <https://doi.org/10.1074/jbc.272.3.1896>
- Wolfe, M.S. 2020. Unraveling the complexity of  $\gamma$ -secretase. *Semin. Cell Dev. Biol.* 105:3–11. <https://doi.org/10.1016/j.semcdb.2020.01.005>
- Zhang, X., R. Hoey, A. Koide, G. Dolios, M. Paduch, P. Nguyen, X. Wu, Y. Li, S.L. Wagner, R. Wang, et al. 2014. A synthetic antibody fragment targeting nicastrin affects assembly and trafficking of  $\gamma$ -secretase. *J. Biol. Chem.* 289:34851–34861. <https://doi.org/10.1074/jbc.M114.609636>
- Zhang, M., A.A. Dillio, R. Khallaf, J.F. Robinson, R.A. Hegele, M. Comishen, C. Sato, G. Tosto, C. Reitz, R. Mayeux, et al. 2019a. Genetic and epigenetic study of an Alzheimer's disease family with monozygotic triplets. *Brain*. 142:3375–3381. <https://doi.org/10.1093/brain/awz289>
- Zhang, T., D. Chen, and T.H. Lee. 2019b. Phosphorylation Signaling in APP Processing in Alzheimer's Disease. *Int. J. Mol. Sci.* 21:209. <https://doi.org/10.3390/ijms21010209>
- Zhang, X., C. Zhang, D. Prokopenko, Y. Liang, W. Han, R.E. Tanzi, and S.S. Sisodia. 2020. Negative evidence for a role of A $\beta$ 11B T27I variant in Alzheimer's disease. *Hum. Mol. Genet.* 29:955–966. <https://doi.org/10.1093/hmg/ddaa017>

## Supplemental material

Table S1 is available online as a separate file and describes large WGS AD datasets.